HHS Public Access

Author manuscript

Biochemistry. Author manuscript; available in PMC 2020 June 12.

Published in final edited form as:

Biochemistry. 2019 December 03; 58(48): 4827–4841. doi:10.1021/acs.biochem.9b00706.

NosP Signaling Modulates the NO/H-NOX-Mediated Multicomponent c-Di-GMP Network and Biofilm Formation in *Shewanella oneidensis*

Lisa-Marie Nisbett[⊥], **Lucas Binnenkade**[§], **Bezalel Bacon**[⊥], **Sajjad Hossain**[#], **Nicholas J. Kotloski**[‖], **Evan D. Brutinel**[‖], **Raimo Hartmann**[†], **Knut Drescher**[†,‡], **Dhruv P. Arora**[#], **Sandhya Muralidharan**[#], **Kai M. Thormann**[§], **Jeffrey A. Gralnick**[‖], **Elizabeth M. Boon**[*,⊥,#,@]

[†]Max Planck Institute for Terrestrial Microbiology, Karl-von-Frisch-Strasse 10, 35043 Marburg, Germany

[‡]Department of Physics, Philipps-Universität Marburg, Renthof 6, 35032 Marburg, Germany

[§]Institute for Microbiology and Molecular Biology, Justus-Liebig-Universität Giessen, D-35392 Giessen, Germany

[‖]Department of Plant and Microbial Biology, University of Minnesota—Twin Cities, St. Paul, Minnesota 55108, United States

[⊥]Graduate Program in Biochemistry and Structural Biology, Stony Brook University, Stony Brook, New York 11794-3400, United States

[#]Department of Chemistry, Stony Brook University, Stony Brook, New York 11794-3400, United States

[@]Institute of Chemical Biology & Drug Discovery, Stony Brook University, Stony Brook, New York 11794-3400, United States

Abstract

[*]**Corresponding Author** Department of Chemistry, Stony Brook University, Stony Brook, NY 11790. elizabeth.boon@stonybrook.edu. Telephone: (631) 632-7945. Fax: (631) 632-7960.

Author Contributions

L.-M.N., L.B., B.B., S.H., N.J.K., E.D.B., R.H., K.D., D.P.A., S.M., K.M.T., J.A.G., and E.M.B. have made major contributions to the acquisition, analysis, or interpretation of the data; L.-M.N., K.M.T., J.A.G., and E.M.B. to the conception or design of the study; and L.-M.N. and E.M.B. to the writing of the manuscript.

Supporting Information

The Supporting Information is available free of charge on the ACS Publications website at DOI: 10.1021/acs.biochem.9b00706.

A table highlighting the strains, plasmids, and primers used in this study, flow-cell biofilms of *S. oneidensis* Δ*nosP*/Δ*hnoX*-GFP, Δ*nahK*/Δ*hnoK*-GFP, Δ*hnoB*-GFP, and Δ*hnoD*-GFP mutant strains and the Δ*hnoD*/p*hnoD*-GFP complement strain (Figure S1A–C), quantitative analysis of attached biofilm, surface coverage, and average thickness parameters of the flow-cell biofilms of *S. oneidensis* wild-type GFP, Δ*hnoB*-GFP, Δ*hnoK*-GFP, Δ*hnoX*-GFP, Δ*hnoD*-GFP, Δ*nahK*-GFP, and Δ*nosP*-GFP mutant strains (Figure S2A–C), autoradiography and SDS–PAGE experiments examining *So*HnoK and *So*NahK autokinase activity (Figure S3A–D), autoradiography and SDS–PAGE experiments with *So*HnoK, *So*HnoB, *So*HnoD, and *So*HnoD D60A (Figure S4A–C), HPLC traces of the c-di-GMP standard and *S. oneidensis* strain samples, MALDI-TOF mass spectrometry experiments with the c-di-GMP standard and *S. oneidensis* strain samples, and a c-di-GMP calibration curve (Figures S5A–E), and NO off kinetics of SoNosP in the presence of 30 mM sodium dithionite NO trap only (Figure S6A,B) (PDF)

Accession Codes

NahK, Q8EE47; NosP, Q8EE48; HnoD, Q8EE49; HnoC, Q8EE50; HnoB, Q8EE51; HnoK, Q8EF48.

The authors declare no competing financial interest.

Biofilms form when bacteria aggregate in a self-secreted exopolysaccharide matrix; they are resistant to antibiotics and implicated in disease. Nitric oxide (NO) is known to mediate biofilm formation in many bacteria via ligation to H-NOX (heme-NO/oxygen binding) domains. Most NO-responsive bacteria, however, lack H-NOX domain-containing proteins. We have identified another NO-sensing protein (NosP), which is predicted to be involved in two-component signaling and biofilm regulation in many species. Here, we demonstrate that NosP participates in the previously described H-NOX/NO-responsive multicomponent c-di-GMP signaling network in *Shewanella oneidensis*. Strains lacking either *nosP* or its co-cistronic kinase *nahK* (previously *hnoS*) produce immature biofilms, while *hnoX* and *hnoK* (kinase responsive to NO/H-NOX) mutants result in wild-type biofilm architecture. We demonstrate that NosP regulates the autophosphorylation activity of NahK as well as HnoK. HnoK and NahK have been shown to regulate three response regulators (HnoB, HnoC, and HnoD) that together comprise a NO-responsive multicomponent c-di-GMP signaling network. Here, we propose that NosP/NahK adds regulation on top of H-NOX/HnoK to modulate this c-di-GMP signaling network, and ultimately biofilm formation, by governing the flux of phosphate through both HnoK and NahK. In addition, it appears that NosP and H-NOX act to counter each other in a push–pull mechanism; NosP/NahK promotes biofilm formation through inhibition of H-NOX/HnoK signaling, which itself reduces the extent of biofilm formation. Addition of NO results in a reduction of c-di-GMP and biofilm formation, primarily through disinhibition of HnoK activity.

Graphical Abstract

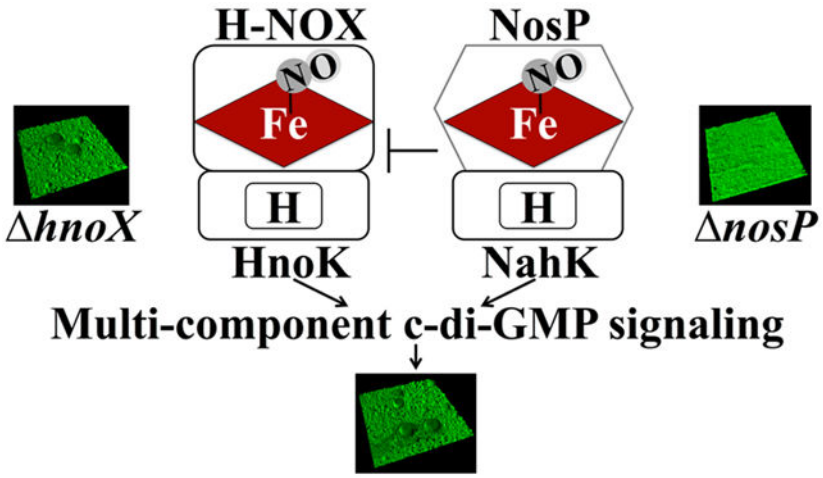

Over the past decade, many research groups have shown that low (approximately nanomolar) concentrations of nitric oxide (NO), a small diatomic gas, regulate biofilm formation.[1] In many bacteria, the molecular basis for this NO-mediated biofilm response has been demonstrated to be ligation of NO to H-NOX (heme-NO/oxygen binding) proteins.[2] Although many bacteria appear to be responsive to NO, only a minority encode an H-NOX domain. Fundamental questions, therefore, remain about the identity of bacterial NO sensors and the molecular mechanisms by which NO regulates biofilm formation in bacteria.

Recently, our lab has identified a novel NO-sensing hemoprotein, which we have named NosP (NO-sensing protein).[3,4] Within bacterial genomes, NosP domains are annotated as

FIST (F-box intracellular signal transduction proteins) or DUF1745 domain-containing proteins, based on their predicted secondary structure.[5] Most NosP sequences are encoded as stand-alone proteins, but some are predicted to be a domain of a larger polypeptide. Many NosP domains are predicted to be involved in two-component signal transduction networks that mediate biofilm formation by way of regulating downstream diguanylate cyclase (c-di-GMP synthase) and/or phosphodiesterase enzymes. c-Di-GMP is a known secondary messenger molecule involved in regulating biofilm formation, among many other important physiological processes, in many bacteria.[6]

NosP domains were only very recently discovered; at present, little about their function is known. Our laboratory has characterized NosP domains from *Pseudomonas aeruginosa, Vibrio cholerae,* and *Legionella pneumophila* and found they are hemoproteins that can bind NO and CO but not molecular oxygen[3,4,7] (Fischer et al., unpublished data). Biochemical characterization of the NosP-associated two-component signaling pathways in these organisms revealed that *Pa*NosP and *Lpg*NosP inhibit the autophosphorylation activities of co-cistronic histidine kinases that had previously been implicated in biofilm formation[3] (Fischer et al., unpublished data). *Vc*NosP was demonstrated to inhibit the autophosphorylation activity of a co-cistronic quorum-sensing histidine kinase VpsS.[4]

Although NosP domains are generally encoded in bacteria that lack H-NOX domains, interestingly, there are a handful of bacteria that possess both putative NO-sensing proteins, the purpose of which is currently unknown. *Shewanella oneidensis* encodes an H-NOX domain (SO_2144) that is co-cistronic with an H-NOX-associated histidine kinase called HnoK (SO_2145). *S. oneidensis* also encodes a NosP domain (SO_2542), which is predicted to be a stand-alone protein co-cistronic with the histidine kinase SO_2543. This protein was previously named HnoS,[8] but we have renamed it NahK for NosP-associated histidine kinase. *So*NahK and *So*HnoK have been previously demonstrated to participate in a multicomponent c-di-GMP signaling network, consisting of the response regulators *So*HnoB (SO_2539), *So*HnoC (SO_2540), and *So*HnoD (SO_2541), that regulates biofilm in response to NO.[8]

In this study, we demonstrate that in *S. oneidensis*, *So*NosP appears to act as a master regulator of the *So*HnoB/*So*HnoC/*So*HnoD multicomponent c-di-GMP signaling network through inhibition of *So*H-NOX/*So*HnoK signaling. It appears that *So*NosP and *So*H-NOX are engaged in a push–pull mechanism; *So*NosP/*So*NahK promotes biofilm formation through inhibition of H-NOX/HnoK signaling, which itself works to reduce the extent of biofilm formation. Addition of NO to this system causes a reduction in c-di-GMP levels, primarily because *So*HnoK activity becomes uninhibited by *So*NosP.

MATERIALS AND METHODS

Materials.

All reagents were purchased at their highest available purity and used as received.

Bacterial Strains and Growth Conditions.

Strains used in this study are listed in Supplemental Table 1. *Escherichia coli* strain DH5α was used for plasmid amplification; *E. coli* WM3064 was used for conjugation, and *E. coli* strain BL21 (DE3) pLysS was used for protein expression and purification. *E. coli* was grown in Lennox broth (LB; 20 g/L) at 37 °C with agitation at 250 rpm. *S. oneidensis* MR-1 was grown in either Lennox broth (LB; 20 g/L) or lactate medium (LM) [0.02% (w/v) yeast extract, 0.01% (w/v) peptone, 10 mM (w/v) HEPES (pH 7.4), 10 mM $NaHCO_3$, and 0.5 mM lactate][9] at 30 °C with agitation at 250 rpm.

Construction of In-Frame Gene Disruption *S. oneidensis* Mutants.

Gene deletions for SO_2144 (Δ*hnoX*), SO_2145 (Δ*hnoK*), SO_2539 (Δ*hnoB*), SO_2541 (Δ*hnoD*), SO_2542 (Δ*nosP*), SO_2543 (Δ*nahK*), SO_2144/SO_2542 (Δ*hnoX*/Δ*nosP*), and SO_2145/SO_2543 (Δ*hnoK*/Δ*nahK*) strains of *S. oneidensis* were prepared using suicide vector pSMV3 and homologous recombination as previously described,[10] using primers found in Supplemental Table 1.

Construction of Gene Disruption *S. oneidensis* Mutant Complementation Plasmids.

hnoD along with 30 bp upstream of *hnoD* and *nosP* along with 200 bp upstream of *nosP* and *nahK* along with 200 bp upstream of *nahK* were each cloned into broad host range plasmid pBBR1MCS-2 and sequenced (Stony Brook DNA Sequencing Facility). Thereafter, the resulting p*hnoD* plasmid was introduced into the Δ*hnoD* mutant strain as previously described,[10] while the p*nosP* and p*nahK* plasmids were introduced into the *S. oneidensis* Δ*nosP* and Δ*nahK* mutant strains, respectively, via electroporation.

Construction of Gene Disruption *S. oneidensis* MR-1 Mutant Complementation Strains.

S. oneidensis Δ*nosP* and Δ*nahK* complemented strains were made as previously described,[10] with slight modifications. Briefly, 5 mL LB cultures of Δ*nosP* and Δ*nahK S. oneidensis* mutant strains were grown overnight (~16 h) at 28 °C. The cultures were then centrifuged for 1 min at 16813*g*, after which the cells were washed once with 0.33 mL of sterile 1 M D-sorbitol (pH 7.59). Next, the cells were resuspended in 0.05 mL of 1 M D-sorbitol and placed on ice. Thereafter, plasmid DNA was introduced into the mutant strains via electroporation using 0.1 cm cuvettes and a BTX model 600 Electro Cell manipulator with a pulse controller (resistance of 200 Ω, capacitance of 25 μFD, voltage of 0.55 kV). After electroporation, the cells were suspended in 0.5 mL of LB and successful p*nosP* and p*nahK S. oneidensis* complemented mutants were selected for on LB agar plates supplemented with 10 μg mL^{-1} kanamycin that were incubated overnight (~16 h) at 30 °C.

Biofilm Cultivation and Image Acquisition.

To enable fluorescence microscopic analysis on biofilms, *S. oneidensis* MR-1 strains constitutively expressing *egfp* were constructed by using a modified Tn7 delivery system.[11] For image acquisition, biofilms were cultivated in LM [10 mM HEPES (pH 7.5), 100 mM NaCl, 0.02% yeast extract, and 0.01% peptone] containing 0.5 mM lactate under hydrodynamic conditions in custom-made three-channel flow cells as previously described.[9,11] Microscopic visualization of biofilms and image acquisition were performed close to the

medium inflow of the flow chamber using an inverted Leica TCS SP5 confocal laser scanning microscope (Leica Microsystems, Wetzlar, Germany) equipped with 10×/0.3 Plan-Neofluar and 63×/1.2 W C-Apochromate objectives. CSLM images were further processed using the IMARIS software package (Bitplane AG, Zürich, Switzerland) and Adobe Photoshop. Image analysis (e.g., determination of surface coverage) was conducted using ImageJ version 1.47, including the LOCI Bio-Formats plugin. Biofilm cultivation and measurements were conducted in triplicate in at least two independent experiments.

Quantitative Analysis of Confocal Laser Microscopy Images.

Whole biofilms were segmented and analyzed with MatLab (Mathworks) using previously described methods.[12,13] Prior to analysis, each biofilm stack was automatically rotated to correct for tilting of the coverslip with respect to the imaging plane. Then, the biofilm was segmented by three-level thresholding[14] where the first class was assigned to background and the remaining ones constitute the biofilm. The total biomass (volume of all biofilm-associated voxels), the surface coverage (fraction of biofilm-associated voxels in the brightest *z*-plane of the image stack), and the average thickness (average thickness of the *z*-projection of the image stack) were determined. Non-surface-attached biomass was excluded from the analysis. Statistical *p* values were obtained using a one-way analysis of variance (ANOVA) in combination with the Tukey–Kramer method.[15]

Extraction and Quantification of c-Di-GMP.

Intracellular c-di-GMP was extracted and quantified as previously described,[16] with slight modifications. Briefly, single wild-type or mutant *S. oneidensis* colonies (not constitutively expressing *egfp*) were cultured in 5 mL of LB overnight (~16 h) at 30 °C with agitation at 250 rpm. The cultures were then diluted to an OD_{600} of 0.07 in LM [10 mM HEPES (pH 7.5), 100 mM NaCl, 0.02% yeast extract, 0.01% peptone, and 0.5 mM lactate] and grown at 30 °C until an OD_{600} of ~0.25–0.3 was attained. To introduce NO, 50 μM diethylamine NONOate (DEA/NO, Cayman Chemicals) was added 20 min before the cells were harvested. The cultures were then pelleted by centrifugation at 2500*g* for 20 min at 4 °C. The supernatants were then discarded, and the pellets were resuspended in 300 μL of icecold extraction buffer (40% methanol, 40% acetonitrile, and 20% Milli-Q water) and incubated on ice for 15 min. Next, the extraction suspensions were heated at 95 °C for 3 min and then cooled on ice for 5 min. The samples were then centrifuged at 17970*g* for 10 min to remove insoluble material, and the supernatant was subsequently transferred to new microcentrifuge tubes. Thereafter, the resulting pellets were extracted twice with 200 μL of extraction buffer at 4 °C omitting the heating step. The supernatants of three extractions were combined and dried using a centrifugal evaporator. The dried pellets were then resuspended in 120 μL of Milli-Q water, and the samples were analyzed using a Shimadzu LC-2010A HT high-performance liquid chromatography system; 60 μL of each sample was injected into a reverse-phase Phenomenex Luna Omega Polar C-18 column (100 mm × 4.6 mm, 5 μm particle size). Separations were conducted in a 15 mM TEAA (triethylammonium acetate) (pH 5.0)/4% methanol solution at a flow rate of 0.5 mL/min. A c-di-GMP calibration curve was generated by running 20 μL of the following triplicate c-di-GMP concentrations under identical high-performance liquid chromatography (HPLC) conditions: 0, 5, 10, 20, and 50 pmol/μL. The picomole amounts of c-di-GMP versus the peak areas were plotted, and a

linear graph with a correlation coefficient, R^2, of 0.98 resulted. c-Di-GMP concentrations were determined by comparing the peak area of the samples to the peak areas of the calibration curve and normalized to the OD_{600} of the culture from which they were extracted. The HPLC peak assigned to c-di-GMP was confirmed by MALDI mass spectrometry (*m*/*z* 689 peak observed, expected mass of 690 g/mol). Each data set was independently obtained a minimum of three times. The mean c-di-GMP concentration relative to the wild-type strain ± one standard deviation (SD) is reported.

Protein Cloning.

SO_2144 (*hnoX*), SO_2145 (*hnoK*), SO_2539 (*hnoB*), SO_2540 (*hnoC*), SO_2541 (*hnoD*), SO_2542 (*nosP*), and SO_2543 (*nahK*) were amplified from *S. oneidensis* genomic DNA using Phusion DNA polymerase (NEB). SO_2144, SO_2539, SO_2540, and SO_2542 were cloned into the pET20b vector and transformed into *E. coli* BL21(DE3) pLysS cells for protein overexpression. BL21(DE3) pLysS SO_2144 transformed bacterial cell cultures were grown in Terrific Broth (12 g of tryptone, 24 g of yeast extract, 4 mL of glycerol, and 100 mL of 0.17 M monobasic potassium phosphate and 0.72 M dibasic potassium phosphate per liter) supplemented with 100 μg mL^{-1} ampicillin and 34 μg mL^{-1} chloramphenicol at 37 °C until an OD_{600} of 0.6 was attained. Overexpression was then induced with 10 μM IPTG at 18 °C for 16 h. BL21(DE3) pLysS SO_2542 transformed bacterial cell cultures were grown in buffered yeast extract (45 g of yeast extract and 100 mL of 0.17 M monobasic sodium phosphate and 0.72 M dibasic sodium phosphate per liter). Twenty micromolar hemin (final concentration) was added at an OD_{600} of 0.3, and overexpression was then induced with 10 μM IPTG at an OD_{600} of 0.6 for 16 h at 16 °C. BL21(DE3) pLysS transformed SO_2539, SO_2540, and SO_2541 bacterial cell cultures were each grown in 2XYT medium (16 g of tryptone, 10 g of yeast extract, and 5 g of sodium chloride per liter) supplemented with 100 μg mL^{-1} ampicillin and 34 μg mL^{-1} chloramphenicol at 37 °C until OD_{600} values of 0.8, 0.5, and 0.8, respectively, were reached. Overexpression of each culture was then induced with 200 μM IPTG for 16 h at 16 °C. SO_2145 was cloned into the pET23a vector and the pT7TEVHMBP1vector, while SO_2543 was cloned into both the pT7TEVHMBP1 vector and the pET20b vector. The constructs were subsequently transformed into BL21(DE3) pLysS cells for protein overproduction. Cultures were grown in 2XYT medium (16 g of tryptone, 10 g of yeast extract, and 5 g of sodium chloride per liter) supplemented with 10 μg mL^{-1} kanamycin and 34 μg mL^{-1} chloramphenicol at 37 °C until the OD_{600} reached 1.0 for the pT7TEVHMBP1 vector constructs or supplemented with 100 μg mL^{-1} ampicillin and 34 μg mL^{-1} chloramphenicol at 37 °C until the OD_{600} reached 0.8 for the pET23a and pET20b vector constructs, and overexpression was induced with 200 μM IPTG for 16 h at 16 °C. His_6-tagged proteins were purified using metal (Ni-NTA) affinity chromatography, and gel filtration was further utilized for *So*NosP (Superdex 200 HiLoad 26/60) only. Protein concentrations were determined using the Bradford assay with BSA as a standard.[17]

Electronic Spectroscopy.

All electronic spectra were recorded against a background of deoxygenated buffer [50 mM Tris (pH 7.5) and 300 mM NaCl] from 250 to 750 nm using a Varian UV/vis Cary-100 spectrophotometer. *So*H-NOX ligation complexes were prepared as previously described[18]

with slight modifications. Briefly, ferrous *So*H-NOX was prepared anaerobically by incubation with 10 mM $Na_2S_2O_4$ for 30 min at ambient temperature. *So*H-NOX was then desalted using a PD-10 column, equilibriated with deoxygenated buffer, and placed in a septum-sealed cuvette for the collection of spectra. NO-bound ferrous *So*H-NOX was then prepared by adding DEA-NONOate to ferrous *So*H-NOX for 30 min. *So*H-NOX was then desalted, and a spectrum was recorded. *So*NosP ligation complexes were prepared as follows. Ferrous *So*NosP was anaerobically prepared via incubation with 60 mM $Na_2S_2O_4$ for 45 min at ambient temperature. *So*NosP was then desalted using a PD-10 column equilibrated with deoxygenated buffer and placed in a septum-sealed cuvette for spectrum collection. NO-bound ferrous *So*NosP was prepared by incubation with DEA-NONOate to ferrous *So*NosP for 30 min. *So*NosP was then desalted, and a spectrum was recorded. CO-bound ferrous *So*NosP was prepared by incubation with excess CO gas to ferrous *So*NosP for 10 min. *So*NosP was then desalted, and a spectrum was recorded.

NO Dissociation Rate.

Fe(II)-NO *So*NosP was prepared (*vide supra*) and treated with deoxygenated buffer saturated with carbon monoxide and a sodium dithionite NO trap (3, 30, and 300 mM sodium dithionite) or with a sodium dithionite NO trap only. The NO trap will function to destroy the NO once it leaves the heme.[19] This will prevent the occurrence of NO rebinding, as it is has been shown that heme proteins have very rapid NO association rates.[20] Dissociation of NO from Fe(II)-NO *So*NosP was then monitored as a function of the Fe(II)-CO *So*NosP complex or as a function of ferrous-unligated *So*NosP formation via periodic scanning of the protein sample using a Varian Cary 100 Bio ultraviolet–visible (UV–vis) spectrophotometer. The NO dissociation rate was then determined by monitoring the increase in the *So*NosP Fe(II)-CO complex absorbance versus time, and the data were subsequently fit to a single exponential or two parallel exponentials of the form $f(x) = A(1 - e^{-kx})$. Each experiment was performed a minimum of six times, and the rates were averaged to obtain an appropriate *So*NosP Fe(II)-NO dissociation rate.[19]

Pull-Down Assays.

Amylose resin was washed in 50 mM HEPES (pH 7.5), 300 mM NaCl, 1 mM PMSF, 2 mM DTT, and 1% Triton X-100. After washing, the His_6-tagged MBP fusion of HnoK and 300 nM His_6-tagged NO-bound ferrous NosP or His_6-tagged MBP fusion of NahK and 100 nM His_6-tagged NO-bound ferrous NosP was added to the resin in a final volume of 500 μL in the same buffer and incubated at 4 °C for 2 h while being gently rocked. The resin was then washed three times with the same buffer and subsequently boiled in 20 μL of SDS buffer. Ten microliters of each reaction mixture was then loaded onto a 12.5% Tris glycine gel for Western blot analysis, and polyclonal anti-His antibodies (Abcam) were used in 5% milk to detect the presence of the His_6-tagged MBP fusion of HnoK, the His_6-tagged MBP fusion of NahK, His_6-tagged NosP, and/or H-NOX proteins. Each experiment was performed in duplicate.

Autophosphorylation Assays.

Kinase autophosphorylation was detected using γ-^{32}P-labeled ATP; 3 μM His_6-tagged MBP fusion of HnoK and NahK was incubated with 5 mM $MgCl_2$, 2 mM ATP, and 40 μCi of

[γ-^{32}P]ATP in reaction buffer [50 mM Tris (pH 7.5) and 300 mM NaCl]. At various time points (0, 5, 10, 20, 30, 60, 90, and 120 min), 10 μL of each reaction mixture was quenched with 3 μL of SDS–PAGE loading buffer. Ten microliters of each sample was then loaded onto a 12.5% Tris-glycine gel to separate the proteins. The gel was then dried overnight (~16 h) (Promega gel drying film), exposed to an autoradiography screen, and scanned using a Typhoon Imager to obtain gel images, which were then analyzed via ImageJ. Each experiment was performed in triplicate.

To determine which response regulator each kinase (HnoK or NahK) kinetically preferred, in the absence of either NO sensor (H-NOX and/or NosP), 3 μM His_6-tagged HnoK or 3 μM His_6-tagged MBP fusion NahK was first preincubated with all three response regulators (HnoB, HnoC, and HnoD, at 3 μM) in reaction buffer [50 mM Tris (pH 7.5) and 300 mM NaCl] supplemented with 5 mM $MgCl_2$ for 10 min. Two millimolar ATP and 10 μCi of [γ-^{32}P]ATP were then added to each reaction mixture, after which 10 μL aliquots were removed and quenched at various time points (0, 0.5, 2, 10, and 15 min for the HnoK experiment and 0, 0.5, 2, 10, 15, 30, and 60 min for the NahK experiment). Each response regulator was also incubated individually with each kinase to assess the maximum level of phosphorylation that could be attained within a set time frame (15 min each for incubation with HnoK and 60 min each for incubation with NahK). Each experiment was performed in duplicate.

Three different experiments were conducted to assess if changes in the levels of HnoB phosphorylation can occur in the presence of HnoD: one in which equimolar amounts of HnoK, HnoB, and HnoD were used, one in which equimolar amounts of HnoK and HnoD were used while HnoB was present in excess, and one in which equimolar amounts of HnoK, HnoB, and mutant HnoD D60A were utilized. To assess if changes in HnoB phosphorylation occur in the presence of equimolar amounts of HnoD or HnoD D60A, 2.5 μM His_6-tagged HnoK, HnoB, and HnoD and 2.5 μM His_6-tagged HnoK, HnoB, and HnoD D60A were first preincubated in reaction buffer [50 mM Tris (pH 7.5) and 300 mM NaCl] supplemented with 5 mM $MgCl_2$ for 10 min. Two millimolar ATP and 10 μCi of [γ-^{32}P]ATP were then added to each reaction mixture, after which 10 μL aliquots were removed and quenched at various time points (0, 0.5, 2, 10, and 15 min). Each response regulator was also incubated individually with HnoK to assess the maximum level of phosphorylation that could be attained within a set time frame (15 min each). Each experiment was performed in duplicate.

To examine changes in HnoB phosphorylation once HnoB was present in excess, 2.5 μM His_6-tagged HnoK, HnoD, and varying concentrations of HnoB (2.5, 5, 12.5, or 25 μM) were first preincubated with reaction buffer [50 mM Tris (pH 7.5) and 300 mM NaCl] supplemented with 5 mM $MgCl_2$ for 10 min. Two millimolar ATP and 10 μCi of [γ-^{32}P]ATP were then added to each reaction mixture, after which 10 μL aliquots were removed and quenched at 15 min. Each response regulator was also incubated individually with HnoK to assess the maximum level of phosphorylation that could be attained within a set time frame (15 min each). Each experiment was performed in duplicate.

To determine the effect of *So*NosP on *So*HnoK and *So*NahK autophosphorylation, 3 μM His_6-tagged MBP fusion of *So*HnoK or *So*NahK was incubated with either Fe(II)-unligated or Fe(II)-NO forms of *So*NosP (15, 30, and 60 μM) in reaction buffer supplemented with 5 mM $MgCl_2$ for 15 min. Two millimolar ATP and 10 μCi of [γ-^{32}P]ATP were added to initiate kinase autophosphorylation. Reactions were then quenched at 30 min for Fe(II)/NosP-HnoK or NO/NosP-HnoK and 45 min for Fe(II)/NosP-NahK or NO/NosP-NahK by the addition of 3 μL of SDS–PAGE loading buffer. Ten microliters of each sample was then loaded onto a 12.5% Tris-glycine gel to separate the proteins. The gels were then dried overnight (~16 h) (Promega gel drying film) and exposed to an autoradiography screen that was subsequently scanned using a Typhoon Imager to obtain gel images, which were analyzed with ImageJ.[21] Each experiment was performed in triplicate.

RESULTS AND DISCUSSION

*So*NosP and *So*NahK Are Essential for Mature Biofilm Formation.

To determine the role of NosP in regulating biofilm formation in *S. oneidensis*, flow-cell biofilms of wild-type and mutant GFP-labeled strains Δ*hnoX*-GFP, Δ*hnoK*-GFP, Δ*nosP*-GFP, Δ*nahK*-GFP, Δ*hnoD*-GFP, Δ*hnoB*-GFP, Δ*nahK*/Δ*hnoK*-GFP, and Δ*nosP*/Δ*hnoX*-GFP were grown and analyzed. Deletion of *hnoX* or *hnoK*, as well as the double kinase knockout strain Δ*nahK*/Δ*hnoK*-GFP, results in no change in biofilm phenotype when compared to the wild-type GFP strain (Figure 1A and Figure S1A). Deletion of both sensors in the Δ*nosP*/Δ*hnoX*-GFP strain appears to result in a hyper-biofilm phenotype at the 24 h time point, but at the 48 h time point, a wild-type-like biofilm phenotype is observed (Figure S1A). A single deletion of either *nosP* or *nahK*, however, results in monolayer biofilms that do not develop into structured mature biofilms, in comparison with the wild-type GFP strain (Figure 1B). Ectopic expression of *nosP* or *nahK* into their respective mutant strains (Δ*nosP*/p*nosP*-GFP and Δ*nahK*/p*nahK*-GFP) yields a restoration of wild-type biofilm (Figure 1C), indicating the biofilm defect was due to a lack of *So*NosP or *So*NahK production.

Quantification of these biofilms reveals that in comparison to the wild-type GFP and other mutant GFP strains, the Δ*nosP*-GFP and Δ*nahK*-GFP strains produce biofilms with more attached biomass, a greater surface coverage, and a greater average thickness after growth for 24 h (Figure S2), but after growth for 48 h, the attached biomass, surface coverage, and average thickness of the Δ*nosP*-GFP and Δ*nahK*-GFP mutant strains are significantly reduced. Overall, however, it is notable that the average attached biomass, surface coverage, and average thickness do not vary dramatically among the various strains tested here. Instead, it appears that *So*NosP and *So*NahK primarily regulate late-stage biofilm architecture.

*So*NosP and *So*NahK Mediate Complex Biofilm Structure through Regulation of Intracellular c-Di-GMP Levels.

Because NahK was previously shown to participate in an NO-responsive multicomponent c-di-GMP signaling network in *S. oneidensis*,[8] we hypothesized that the observed biofilm defects in the Δ*nosP* and Δ*nahK* mutant strains (Figure 1B) may correlate with decreased intracellular c-di-GMP concentrations. Quantification of cellular c-di-GMP levels from

cultures grown in the absence of NO revealed that deletion of *hnoX*, *hnoK*, and *hnoK/nahK* results in c-di-GMP concentrations that are comparable to those of the wild-type MR-1 strain grown in the absence of NO (Table 1). This is expected, as the biofilm images of these strains indicate no phenotype (Figure 1A and Figure S1A).

Cultures of the single deletions of either *nosP* or *nahK*, or the double sensor deletion *nosP*/*hnoX*, grown in the absence of NO, however, result in significantly decreased ($p \leq 0.05$) c-di-GMP levels in comparison to that of the wild-type MR-1 strain grown in the absence of NO (Table 1). Plasmid complementation (Δ*nosP*/*pnosP* and Δ*nahK*/p*nahK*) results in a restoration toward MR-1 wild-type cellular c-di-GMP levels (Table 1). For Δ*nosP* and Δ*nahK*, this is the expected result based on the corresponding biofilm phenotype (Figure 1B,C). For the double mutant Δ*nosP*/Δ*hnoX*, the biofilm images appear to indicate a wild-type-like biofilm by 48 h (Figure S1A), so significantly reduced c-di-GMP levels were not necessarily expected. The time scale of biofilm development in Δ*nosP*/Δ*hnoX* is altered relative to that of the wild type, so perhaps this difference is reflected in our c-di-GMP measurements. It is also possible that the *So*NosP/*So*H-NOX signaling pathway could be primarily functioning through the modulation of local, but not global, c-di-GMP concentrations, which is an important caveat in the interpretation of the measurements of global c-di-GMP concentrations reported here.

*So*NosP and *So*NahK Regulate c-Di-GMP Signaling through *So*HnoB, *So*HnoC, and *So*HnoD.

The data presented above suggest intracellular c-di-GMP concentrations affect complex biofilm architecture and that *So*NosP and *So*NahK are involved in mediating this process. Consequently, on the basis of these findings, as well as the model previously published for this *S. oneidensis* multicomponent c-di-GMP signaling pathway,[8] we propose a revised model in which *So*NosP is a regulator of the *So*H-NOX/*So*HnoK multicomponent c-di-GMP signaling network (Figure 2).

We propose *So*NosP to be at the top of the pathway, because it appears that *So*NosP is actively inhibiting the *So*H-NOX/*So*HnoK pathway in the wild-type strain, such that deletion of either *hnoX* or *hnoK* has no effect on c-di-GMP concentrations (Table 1) and therefore no effect on biofilm formation (Figure 1A). When *So*NosP is removed, however, a biofilm formation defect is observed after growth for 24 h, presumably due to altered c-di-GMP signaling downstream of *So*NahK and *So*HnoK through the activities of three cognate response regulators. Each of these response regulators has previously been shown to be responsive to phosphorylation by *So*NahK and *So*HnoK. The three response regulators are *So*HnoB, an EAL-type c-di-GMP phosphodiesterase; *So*HnoD, a degenerate HD-GYP-type c-di-GMP phosphodiesterase; and *So*HnoC, an HtH-type transcription factor.[8] It is also possible that *So*H-NOX and *So*NosP function in parallel at different time points during biofilm formation; perhaps *So*H-NOX functions earlier than *So*NosP in biofilm formation, such that biofilms formed by Δ*nosP* are similar to the wild type at early time points yet are deficient at later time points. Δ*hnoX* appears to be similar to the wild type at all time points [there are slightly larger, but insignificant ($p > 0.5$), average differences in the biofilm at 24 h (Figure S2)]; however, so we favor a model in which *So*NosP inhibits *So*H-NOX signaling.

The phenotypes of our *hnoD* and *hnoB* deletion mutants are consistent with the inhibition model. Deletion of *hnoB* does not affect the biofilm phenotype or c-di-GMP levels when compared to the wild-type GFP and MR-1 strains, respectively (Figure S1B, Figure S2, and Table 1). Interestingly, we do not observe hyper-biofilm in the Δ*hnoB* mutant. *S. oneidensis* has many other c-di-GMP cyclases and phosphodiesterases[22] that may be compensating for the loss of *hnoB* activity, preventing biofilm dispersal in the absence of a dispersal signal. Alternatively, as proposed, NosP inhibition of the H-NOX pathway, as well as HnoD inhibition of HnoB activity directly, likely results in HnoB inhibition under basal conditions, so its deletion has no apparent phenotype. Deletion of *hnoD* is consistent with our model and results in the deletion of *hnoB*. Δ*hnoD* results in microcolony biofilms that do not develop into complex mature wild-type biofilms after growth for 48 h (Figure S1C). Ectopic complementation of *hnoD* yields a restoration of the wild-type GFP biofilm phenotype (Figure S1C), signifying that the arrest of biofilm at the microcolony phase is due to the lack of expression of *So*HnoD. Deletion of *hnoD* does not significantly affect the attached biomass, surface coverage, or average thickness of the biofilm (Figure S2), nor does it result in a significant reduction in c-di-GMP levels and/or concentrations (Table 1). It has previously been shown that *So*HnoD can competitively inhibit the phosphorylation (and therefore decrease the c-di-GMP phosphodiesterase activity) of the response regulator *So*HnoB;[8] thus, it is probable that a lack of *So*HnoD leads to the increased EAL phosphodiesterase activity of *So*HnoB and therefore a decreased level of biofilm formation over time. It follows, thus, that *So*HnoD may function to fine-tune the activity of *So*HnoB during the transition from micro- to macrocolonies during biofilm development. Perhaps this fine-tuning is a local effect that is reflected in global c-di-GMP levels, or perhaps *So*HnoD has an additional function that has not yet been described.

This model may also explain why the double sensor deletion mutant (Δ*nosP*/Δ*hnoX*-GFP) has a mild phenotype. When the kinases are completely unregulated, *So*HnoD may be phosphorylated earlier in biofilm development than it ought to be, which may remove its fine regulation of *So*HnoB activity, thus increasing phosphodiesterase activity in early biofilm growth. If this is the case, the phenotype of a double kinase deletion (Δ*nahK*/Δ*hnoK*-GFP) can also be explained; in the absence of either kinase, *So*HnoD and *So*HnoB would both be unphosphorylated, and thus, *So*HnoB would have no c-di-GMP phosphodiesterase activity, leading to biofilm accumulation.

We next set out to biochemically investigate our model (Figure 2) and determine the molecular details by which *So*NosP and *So*NahK may be regulating complex biofilm formation in *S. oneidensis*.

*So*HnoK and *So*NahK Exhibit *in Vitro* Kinetic Preferences for Different Response Regulator Proteins in the Absence of H-NOX and NosP.

To understand the activities of *So*HnoK and *So*NahK in the absence of *So*H-NOX and *So*NosP, as is presumably the case in the mutants Δ*nosP*-GFP, Δ*hnoX*-GFP, and Δ*nosP*/Δ*hnoX*-GFP, we first studied their activities in isolation. Each of these kinases has been previously purified, demonstrated to be active, and shown to be capable of transferring phosphate to each of the three response regulators (*So*HnoB, *So*HnoC, and *So*HnoD).[8] We

repeated those experiments as part of this study (Figure 3 and Figure S3). Consistent with previously published data,[18,23] we find that *So*HnoK, in the presence of ATP, displays a time-dependent increase in its level of autophosphorylation (Figure S3A,B), with the linear range of autokinase activity occurring up to 30 min (Figure S3B). *So*NahK was also found to exhibit time-dependent autophosphorylation (Figure S3C,D) with its linear range of activity occurring up to 60 min (Figure S3D). Because *So*HnoK presumably is autophosphorylated more quickly than *So*NahK, we can assume that this difference in autokinase activity could have implications not only for which kinase is predominately active *in vivo* but also for which response regulator(s) becomes phosphorylated, thus leading to changes in c-di-GMP levels *in vivo*.

To determine if there is an association between kinase autophosphorylation and changes in biofilm formation due to potential differences in response regulator protein(s) phosphorylation, we conducted an *in vitro* phosphotransfer response regulator competition experiment. In this experiment, each kinase was incubated with all three response regulators (*So*HnoB, *So*HnoC, and *So*HnoD) simultaneously, and phosphotransfer was monitored over time to determine which response regulator preferentially receives phosphate from each histidine kinase (*So*HnoK and *So*NahK). From this experiment, we found that *So*NahK displays a time-dependent kinetic preference for phosphorylation of the HtH domain-containing response regulator *So*HnoC when all three response regulators are present *in vitro* [Figure 3A (lanes 2–8) and Figure 3B (lanes 2–6)]. *So*HnoK exhibits a time-dependent kinetic preference for phosphorylation of *So*HnoD, the HD-GYP-domain-containing response regulator, when all three response regulators are present *in vitro*.

To ensure that the observed kinase/response regulator preferences described above are not due to significant differences in individual rates of phosphotransfer between the kinase and the individual response regulator proteins, or due to differences in protein loading during the experiments, each response regulator was incubated separately with either *So*NahK or *So*HnoK and the phosphorylation results were analyzed. Each response regulator was observed to be intensely phosphorylated when individually incubated with either kinase [Figure 3A (lanes 9–11) and Figure 3B (lanes 7–9)], and the Coomassie gels revealed that protein loading was consistent throughout each experiment (bottom panels in each part of Figure 3). Thus, from these experiments, we can conclude that *So*HnoK exhibits a kinetic preference for *So*HnoD, whereas *So*NahK preferentially transfers phosphate to *So*HnoC (these preferences are indicated by the darker lines in Figure 8A).

Interestingly, *So*HnoD was previously demonstrated to inhibit the c-di-GMP phosphodiesterase activity of *So*HnoB when unphosphorylated. This inhibition is relieved, however, when *So*HnoD becomes phosphorylated.[8] Because our phosphotransfer profiling experiment reveals that *So*HnoK preferentially transfers phosphate to *So*HnoD, we wanted to further understand how changes in phosphorylation of *So*HnoB in the presence of *So*HnoD could be linked to changes in biofilm formation. Consequently, we conducted three different phosphotransfer profiling experiments. In the first, equimolar concentrations of *So*HnoK, *So*HnoB, and *So*HnoD were incubated together. In the second, equimolar concentrations of *So*HnoK and *So*HnoD were incubated with increasing concentrations of *So*HnoB. In the third, equimolar concentrations of *So*HnoK, *So*HnoB, and a mutant form of

*So*HnoD that is incapable of receiving phosphate (D60A) were incubated together. From these experiments, we found that irrespective of whether *So*HnoB was present in excess, the phosphorylation levels of *So*HnoB were consistently decreased in the presence of *So*HnoD [Figure S4A (lanes 2–6) and Figure S4B (lanes 2–5)]. In the presence of the *So*HnoD D60A mutant, however, a time-dependent increase in the level of *So*HnoB phosphorylation was observed [Figure S4C (lanes 2–6)].

On the basis of these data, we conclude that *So*HnoK prefers to phosphorylate *So*HnoD before *So*HnoB. It has been established that histidine kinase proteins typically display an *in vitro* kinetic preference for their *in vivo* cognate response regulator protein(s).[24-27] This kinetic difference in phosphorylation of *So*HnoB and *So*HnoD must thus be important for the timing of events during biofilm development and dispersal. Phosphorylation of *So*HnoD would remove some inhibition of *So*HnoB before *So*HnoB itself becomes phosphorylated (and therefore a fully active c-di-GMP phosphodiesterase),[8] perhaps resulting in stepwise upregulation of *So*HnoB activity and a decreased level of biofilm accumulation (or an increased level of biofilm dispersal), under conditions where *So*HnoK is active. This interpretation is consistent with our c-di-GMP extraction data (Table 1) and biofilm results (Figure 1). A wild-type-like biofilm phenotype is observed in all strains except the Δ*nosP*-GFP and Δ*nahK*-GFP mutant strains (Figure 1), presumably due to NosP/NahK inhibition of the whole network. This suggests that under basal conditions, HnoK has low activity, resulting in primarily dephosphorylated HnoD and HnoB, leading to decreased c-di-GMP phosphodiesterase activity and an increased level of biofilm formation. More specifically, in the Δ*nahK*-GFP mutant strain, HnoK is presumably the only kinase regulating HnoB and HnoD, which leads to a low level of biofilm accumulation, consistent with increased HnoB phosphodiesterase activity. Furthermore, these results also suggest that in the Δ*nosP*-GFP strain, HnoB has increased activity at 48 h (and perhaps decreased activity at 24 h), possibly due to increased HnoK activity in the absence of NosP.

*So*NosP Displays Ligand Binding Properties That Are Consistent with a NO Sensor.

*So*NahK and *So*HnoK are histidine kinases, proteins that are members of a signaling system that bacteria use to sense, detect, and respond to various environmental stimuli, termed a two-component signaling network.[28] Histidine kinases of this signaling system typically possess a sensory domain that enables them to detect stimuli and ultimately alter their autophosphorylation state and thus influence their His-Asp phosphorelay to downstream response regulator proteins.[29] Many two-component signaling systems, however, can deviate from the aforementioned architecture in that the histidine kinases can lack sensory domains. In these alternate systems, the sensory domains are commonly replaced by an accessory protein that functions to directly detect the stimulus and convey the information to the histidine kinases via protein–protein interaction.[30,31]

Both *So*NahK and *So*HnoK lack sensory domains, but both are co-cistronic with a sensory protein, *So*NosP and *So*H-NOX, respectively. In previous studies, it has been demonstrated that *So*HnoK autokinase activity is regulated in an NO/*So*H-NOX-dependent manner,[8,18,32] while the regulator of *So*NahK autokinase activity was unknown.[8] Although co-expression does not always imply functional interaction, given that the *So*NosP domain is predicted to

be co-cistronic with *So*NahK and is bioinformatically predicted to be a homologue of the NosP hemoprotein in *P. aeruginosa,*[3] we hypothesized that like *Pa*NosP, *So*NosP may be a hemoprotein sensor that regulates *So*NahK autophosphorylation activity in a NO-dependent manner.

Indeed, we have shown purified *So*NosP binds heme (Figure 4A). Heme, a prosthetic group in many proteins,[33] absorbs light in the UV–vis region of the electromagnetic spectrum (with a high extinction Soret band in the range of 380–500 nm and Q-band absorbances in the range of 500–750 nm).[34] These absorbance bands are sensitive to the oxidation and ligation state of the heme cofactor, as well as the local environment of protein in which it is embedded. Upon anaerobic treatment of *So*NosP with sodium dithionite, the ferrous form of *So*NosP is observed with a Soret maximum at 417 nm and split α/β bands at 552 and 524 nm (Figure 4A, black solid line). Treatment of the ferrous complex with DEA-NONOate (a compound that releases NO in aqueous solution at pH <7[35]) results in an NO-bound ferrous complex with a Soret maximum at 397 nm (Figure 4A, black dashed line), and addition of CO gas to ferrous *So*NosP shifted the Soret maximum to 416 nm (Figure 4A, gray solid line).

To support the hypothesis that *So*NosP may be a NO sensor, we measured the NO dissociation rate constant using a standard CO/dithionite trap,[19] to get a sense of the affinity of *So*NosP for NO. A k_{off}(NO) of (2.25 ± 0.5) × 10^{-4} s^{-1} was measured for *So*NosP (Table 2), independent of CO and dithionite concentration (Figure 4 and Figure S6). Although the NO association rate constant of *So*NosP has yet to be determined, it is likely that the association rate is in the range of 10^4 – 10^8 M^{-1} s^{-1}, a range that is consistent with measured association rate constants for the association of other diatomic gas molecules with heme proteins.[39] As a result, it is likely that NosP binds NO with nanomolar or lower affinity. These ligand binding properties of *So*NosP are comparable to those of *Pa*NosP and characterized bacterial NO-sensing H-NOX proteins (Table 2), substantiating our hypothesis that *So*NosP is a NO-sensing hemoprotein.

NO-Bound *So*NosP Interacts with *So*HnoK and *So*NahK.

*So*NosP is predicted to be in the same operon with the histidine kinase *So*NahK, suggesting that *So*NosP and *So*NahK could be functional partners. In addition, as suggested by our mutagenesis studies discussed above (Figure 1), we hypothesize that *So*NosP may interact with *So*H-NOX or *So*HnoK to inhibit *So*H-NOX signaling and act as the master regulator of the multicomponent c-di-GMP signaling pathway and therefore complex biofilm formation in *S. oneidensis* MR-1 (Figure 2). To test these hypotheses, we investigated the interaction of NO-bound NosP with both NahK and HnoK using pull-down assays. Using a His_6-tagged-MBP fusion of *So*NahK as bait, we found that *So*NosP was pulled down by *So*NahK (Figure 5A, lane 3) but not by His_6-tagged-MBP (Figure 5A, lane 2) or amylose resin only (Figure 5A, lane 1).

This result supports our hypothesis, as it demonstrates that *So*NosP and *So*NahK are binding partners.

Furthermore, and perhaps more surprisingly, upon incubation with the His_6-tagged MBP fusion of *So*HnoK, pull down of *So*NosP was also observed (Figure 5B, lane 3). *So*HnoK is in the same operon as *So*H-NOX, and *So*H-NOX has been shown to interact with and regulate *So*HnoK phosphorylation.[8,18,32] Nevertheless, our findings indicate that *So*NosP also interacts with *So*HnoK, suggesting a molecular-level mechanism by which *So*NosP may modulate *S. oneidensis* biofilm formation through regulation of both *So*NahK and *So*HnoK autophosphorylation activities. *So*NosP would thus regulate the flux of phosphate through the three associated response regulator proteins (*So*HnoB, *So*HnoC, and *So*HnoD), thereby regulating intracellular c-di-GMP levels and biofilm formation in this bacterium, consistent with our biofilm data described above.

Ferrous and NO-Bound *So*NosP Complexes Inhibit *So*HnoK and *So*NahK Autophosphorylation Activities.

Our findings described above demonstrate that *So*NosP is a NO binding protein that interacts with both *So*NahK and *So*HnoK. Our biofilms, however, were grown in the absence of NO. Because the intracellular environment of a bacterial cell is known to be a reducing environment,[40,41] we assume that *So*NosP predominantly existed in the Fe(II)-unligated form during the biofilm experiments. Consequently, we wanted to assess if *So*NosP, when present in either the Fe(II)-unligated form or the Fe(II)-NO complex, could regulate *So*NahK and/or *So*HnoK autokinase activities. As such, we separately incubated each histidine kinase (*So*NahK or *So*HnoK) with varying concentrations of *So*NosP (5-, 10-, or 20-fold excess) as either the Fe(II)-unligated or Fe(II)-NO complex and observed *So*NahK and *So*HnoK autophosphorylation activities (Figures 6 and 7).

*So*NosP as the Fe(II)-unligated complex inhibits both *So*HnoK and *So*NahK in a dose-dependent manner (Figure 6), but at all concentrations tested, *So*NosP inhibits *So*NahK (approximately 50–65% inhibition over the concentrations tested) to a greater extent than *So*HnoK (approximately 15–40% inhibition over the concentrations tested). We also observed inhibition of both *So*NahK and *So*HnoK autophosphorylation activities when *So*NosP was present in the NO-bound form (Figure 7). The effect of Fe(II)-NO *So*NosP on *So*HnoK activity, however, is relatively weak; we observed a maximum of ~35% inhibition *So*HnoK activity at the highest *So*NosP concentration tested. NO-bound *So*NosP inhibits *So*NahK to a greater extent than *So*HnoK, the inhibition reaching ~50% when NO-bound *So*NosP was present in 20-fold excess. The relative mRNA expression levels of the *So*NosP- and *So*H-NOX-containing operons are similar,[42] suggesting that all of these proteins are present at similar concentrations in *S. oneidensis*. Thus, we conclude that the observed inhibitory effects of *So*NosP on *So*HnoK are physiologically relevant.

It is not surprising that *So*NosP more strongly inhibits *So*NahK than *So*HnoK. *So*NosP is predicted to be co-cistronic with *So*NahK, and our pull-down data (Figure 5) suggest *So*NosP binds *So*NahK more tightly than *So*HnoK. What is somewhat surprising, however, is that assuming that under basal conditions *So*NosP is present in the Fe(II)-unligated state, the binding of NO to *So*NosP appears to relieve inhibition of both kinases, but interestingly, *So*HnoK is more uninhibited than *So*NahK. These data thus predict that in the presence of small amounts of NO, *So*HnoK should become active, leading to phosphorylation of

*So*HnoB, decreased c-di-GMP concentrations, and biofilm dispersal (this preference is indicated by the darker line in Figure 8B).

We did not study the regulation of *So*NahK by *So*H-NOX because there is no evidence that the two proteins interact.[8] The regulation of *So*HnoK by *So*H-NOX has been studied. Although *So*HnoK is known to form a complex with *So*H-NOX,[18,32] appreciable inhibition of *So*HnoK autokinase activity is not observed without a significant stoichiometric excess of NO-bound *So*H-NOX; the greatest inhibitory effect (~90%) was observed with a 100-fold excess of *So*H-NOX over *So*HnoK.[18] In separate published studies from the same group, Fe(II)-unligated *So*H-NOX has both been shown to have no effect on HnoK activity[18] and to increase *So*HnoK activity.[32] In either case, these biochemical data suggest that the activity of *So*HnoK is not sensitively dependent on *So*H-NOX, which, on one hand is surprising, as H-NOX has been shown to sensitively regulate enzyme activity in other systems.[10,29,43-45] One the other hand, however, this is consistent with our data demonstrating that *So*NosP plays an important role in the regulation of *So*HnoK activity (Figures 6 and 7). Taken together, these biochemical data support a new model in which *So*NosP inhibits the downstream activities of *So*HnoK, *So*HnoB, *So*HnoC, and *So*HnoD and in which this inhibition is relieved upon NO binding.

NO Results in Decreased c-Di-GMP Levels in *S. oneidensis* through Modulation of *So*HnoK and *So*NahK Activities.

To test the prediction that binding of NO to *So*NosP results in *So*HnoK activation, in turn leading to phosphorylation of *So*HnoB, decreased c-di-GMP concentrations, and biofilm dispersal, we quantified the effect of NO (~50 nM) on intracellular c-di-GMP concentrations in wild-type *S. oneidensis* MR-1 and mutant strains (Table 1). Indeed, we found that exposure to NO results in a significant decrease (~40%) in intracellular c-di-GMP levels in the MR-1 strain, relative to the same strain grown in the absence of NO (Table 1). Mutant strains *nosP* and *nahK* grown in the presence of NO do not have significantly lower ($p > 0.05$) c-di-GMP concentrations than the same strains grown without NO, but plasmid complementation of these mutants results in wild-type-like reductions in c-di-GMP levels in response to NO exposure. This is in accordance with our biofilm and biochemical data discussed above; addition of NO to wild-type cells should result in increased *So*HnoK and *So*HnoB activities, which is the same phenotype seen upon deletion of *So*NosP or *So*NahK (Figure 1 and Table 1). In other words, addition of NO to wild-type *S. oneidensis* should have the same effect as removal of *So*NosP or *So*NahK.

We also see no statistically significant effect of the addition of NO on the amount of c-di-GMP produced in the *hnoX, hnoK, hnoB,* and *hnoX/nosP* mutant strains, relative to those same strains grown without NO addition (Table 1). Overall, these data nicely fit our model. The *hnoX/nosP* mutant lacks both NO sensors, which should render the cells insensitive to NO. Likewise, because NO/*So*H-NOX does not appear to sensitively regulate the activity of *So*HnoK,[18,32] deletion of *hnoX* should not significantly alter the NO response. Deletion of *hnoK* should result in inactive *So*HnoB and thus increased or unchanged c-di-GMP levels; thus, the addition of NO to this system is not expected to have an effect because NO acts upstream of the deletion.

Deletion of *hnoK/nahK* or *hnoD* results in a significant decrease in cellular c-di-GMP concentrations in the presence of NO (Table 1), in comparison to those same cultures grown without NO. Interestingly, these are the three proteins that regulate the activity of *So*HnoB, which, presumably, is primarily controlling the c-di-GMP output of this network. We predict that *So*HnoD acts to fine-tune *So*HnoB; thus, the *hnoD* mutant strain should result in less tightly regulated *So*HnoB. Addition of NO to this mutant presumably acts through *So*NosP/*So*NahK to fully activate *So*HnoB, resulting in a decreased level of c-di-GMP accumulation, which is indeed what we observe (Table 1).

In the double kinase mutant (Δ*hnoK*/Δ*nahK*), all three response regulators, *So*HnoB, *So*HnoC, and *So*HnoD, should be dephosphorylated, leading to inhibited *So*HnoB and thus unchanged c-di-GMP and biofilm levels, in comparison to those of the wild type, which is what we observe in the absence of NO (Figure S1A and Table 1). Upon addition of NO to this mutant, we would expect no effect because NO should act upstream of this mutation, but that is not what we observe here. This mutant is the only strain we studied that has significantly reduced c-di-GMP levels grown in the presence of NO relative to the wild type grown in the presence of NO, which is not easily understood on the basis of our model. These results may indicate that an additional, uncharacterized NO-responsive element can interact with this c-di-GMP signaling network. Additional NO-responsive candidates could possibly include SO_2544 and SO_2545, genes for two additional kinases that are situated in operons rich in two-component signaling proteins and in the same regions of the *S. oneidensis* genome as the NosP/H-NOX c-di-GMP signaling network.[8] SO_2544, however, has been demonstrated to engage in phosphate flux with a CheY response regulator (SO_2547);[8] in addition, SO_2544 is predicted to be membrane-associated, a feature that is inconsistent with what is currently understood about bacterial NO signaling in the context of two-component signaling histidine kinase proteins, although not disqualifying. Like SO_2544, SO_2545 has been demonstrated to transfer phosphate preferentially to SO_2547. Interestingly, this kinase may weakly engage in phosphate flux to HnoB, HnoC, and HnoD[8] and is predicted to be cytosolic. As a result, it is possible that SO_2545 can compensate for the absence of *So*HnoK and *So*NahK to regulate the c-di-GMP output from this signaling network in the presence of NO. Further studies need to be conducted to determine if this is indeed the case.

Our NO-dependent intracellular c-di-GMP data collectively suggest that in the presence of NO a decreased biofilm phenotype should be observed in wild-type *S. oneidensis.* It is important to note, however, that there could be differences in the response of a biofilm to NO that are not captured in our c-di-GMP extraction data. Biofilms are complex and heterogeneous.[48] The c-di-GMP data reported here were chemically extracted from planktonically grown cells and reflect changes in global, not local, c-di-GMP concentrations. While it has been demonstrated that c-di-GMP levels from planktonically grown cells correlate well with flow-cell biofilm data in this organism,[47] we acknowledge that planktonic growth is different from flow-cell biofilm growth and that our method reports on the average c-di-GMP concentrations present in the bacteria and not the dynamic c-di-GMP concentration changes that occur during a biofilm life cycle.[48] Due to these caveats, our findings can be utilized to suggest, rather than definitely describe, how the intracellular c-di-GMP concentration may change in a *S. oneidensis* biofilm upon exposure to NO.

A New Model for NO/*So*NosP Modulation of the *So*H-NOX/*So*HnoK Multicomponent c-Di-GMP Network.

When all of our data are considered together, we are able to expand our model to include the effect of NO on the *S. oneidensis* c-di-GMP signaling network (Figure 8). We propose that in wild-type *S. oneidensis*, the H-NOX/HnoK pathway [in the absence of NO (Figure 8A)] is inhibited by the action of the Fe(II)-unligated NosP/NahK complex. The data that support this model are as follows. In the wild type, as well as the Δ*hnoX*, Δ*hnoK*, and Δ*hnoB* strains, *So*HnoK activity is inhibited (Figure 6A; or absent, as in Δ*hnoK*) and thus *So*HnoD is largely dephosphorylated (Figure 3B), leading to *So*HnoB inhibition[8] (or absence, as in Δ*hnoB*), bringing about low c-di-GMP phosphodiesterase activity, high c-di-GMP levels (Table 1), and wild-type biofilm formation (Figure 1 and Figure S1).

In the Δ*nosP* mutant, it is reasonable to assume that a large percentage of *So*HnoK is active [because it is not strongly inhibited by *So*H-NOX[18,32] and *So*NosP inhibition is relieved (Figure 6A)] and therefore actively transferring phosphate primarily to *So*HnoD, but also to *So*HnoB (Figure 3B). Because phosphorylated *So*HnoD no longer inhibits *So*HnoB, we would expect *So*HnoB to exhibit increased c-di-GMP phosphodiesterase activity, which in turn could lead to the bacteria having low intracellular c-di-GMP concentrations and therefore decreased levels of biofilm formation, as we have observed (Figure 1 and Table 1). Additionally, because *So*NosP more tightly binds to *So*NahK than *So*HnoK (Figure 5) and inhibits the activity of *So*NahK to a greater extent than *So*HnoK (Figure 6), it is not unreasonable to assume that *So*NosP and *So*NahK predominantly exist and function as a complex *in vivo* that acts to inhibit HnoK autokinase activity. Consequently, perhaps the Δ*nahK* strain, like the Δ*nosP* strain, results in an increase in *So*HnoK activity, and thus increased *So*HnoB activity and decreased c-di-GMP and biofilm levels, similar to those of the Δ*nosP* mutant.

When NO is present (Figure 8B), we propose that the *So*H-NOX/*So*HnoK complex becomes uninhibited by the action of the Fe(II)-NO/*So*NosP/*So*NahK complex. We have demonstrated that *So*NosP inhibits the activities of both *So*NahK and *So*HnoK in the Fe(II)-unligated and Fe(II)-NO complexes (Figures 6 and 7), and *So*H-NOX can also inhibit the activity of *So*HnoK;[18,32] however, significantly, the greatest difference in the activity of either kinase upon addition of NO is the uninhibition of *So*HnoK by NO-bound *So*NosP (Figures 6 and 7). Thus, addition of NO should activate *So*HnoK, leading to an increased flux of phosphate to both *So*HnoD and *So*HnoB (Figure 3), resulting in increased *So*HnoB c-di-GMP phosphodiesterase activity, decreased intracellular c-di-GMP levels (Table 1), and subsequent decreased levels of biofilm formation.

Furthermore, due to the absence of three-dimensional biofilm architecture in the Δ*nosP* and Δ*nahK* mutant strains, it is highly possible that through the fine-tuning of *So*HnoB activity (via the combined efforts of *So*HnoK, *So*HnoD, and the *So*NosP/*So*NahK complex) and therefore tight regulation of intracellular c-di-GMP concentrations, *So*NosP/*So*NahK may function as a master regulator of complex biofilm formation in *S. oneidensis.* Complex biofilm formation has previously been linked to flagellar rotation in this bacterium,[9] a process that is known to be inhibited by elevated intracellular c-di-GMP levels.[46] Furthermore, it has been shown that removal of key components of the *mxdABCD* gene

cluster (*mxd*A and *mxd*B) leads to intracellular c-di-GMP concentration changes and monolayer biofilm phenotypes,[47] results that are reminiscent of the monolayer biofilm phenotypes we observe in the Δ*nosP* and Δ*nahK* mutants. Thus, it is possible that the *So*NosP/*So*NahK network may function upstream of, or in parallel with, the *mxdABCD* gene cluster, such that Δ*nosP* and Δ*nahK* result in a decreased *mxdABCD* gene cluster expression level or activity, decreased c-di-GMP levels, increased flagellar rotation, and a decreased level of biofilm formation. Future experiments are needed to validate if this is indeed the case.

CONCLUSIONS

We have presented data demonstrating that *So*NosP/*So*NahK and the associated multicomponent c-di-GMP signaling network are essential for regulating mature biofilm formation in *S. oneidensis*, suggesting that the *So*NosP/*So*NahK complex may function as a master regulator of NO-mediated biofilm formation. The molecular mechanism responsible for this regulation appears to be fine-tuning of HnoB activity through the combined efforts of *So*HnoD, *So*HnoK, and the *So*NosP/*So*NahK complex. This study also further solidifies the role of NosP as a NO-sensing hemoprotein that can modulate biofilm formation in various bacteria, including those that encode both H-NOX and NosP domains.

Supplementary Material

Refer to Web version on PubMed Central for supplementary material.

ACKNOWLEDGMENTS

The authors thank Dr. Roger Johnson (Stony Brook University) for his helpful advice.

Funding

This work was supported by the Stony Wold-Herbert Fund, the National Science Foundation (Grant CHE-1607532 to E.M.B.), and the National Institutes of Health (Grant GM118894-01A1 to E.M.B. and Grant T32GM092714 to L.-M.N.).

ABBREVIATIONS

NO
nitric oxide

c-di-GMP or cyclic-di-GMP
bis(3′–5′)-cyclic dimeric guanosine monophosphate

So
S. oneidensis

H-NOX
heme-nitric oxide/oxygen binding domain-containing protein

NosP
nitric oxide-sensing protein

HnoK
H-NOX-associated histidine kinase

NahK
NosP-associated histidine kinase

HnoB
EAL-type c-di-GMP phosphodiesterase

HnoC
HtH-type transcription factor

HnoD
degenerate HD-GYP-type c-di-GMP phosphodiesterase

IPTG
isopropyl β-D-1-thiogalactopyranoside

PMSF
phenylmethanesulfonyl fluoride

BSA
bovine serum albumin

DTT
dithiothreitol

CSLM
confocal scanning laser microscope

PVC
polyvinyl chloride

OD
optical density

MBP
maltose binding protein

Tris
tris(hydroxymethyl)aminomethane

DEA-NONOate
diethylamine NONOate

SDS–PAGE
sodium dodecyl sulfate–polyacrylamide gel electrophoresis

REFERENCES

(1). Arora DP, Hossain S, Xu Y, and Boon EM (2015) Nitric Oxide Regulation of Bacterial Biofilms. Biochemistry 54, 3717–3728. [PubMed: 25996573]

(2). Muralidharan S, and Boon EM (2012) Heme Flattening Is Sufficient for Signal Transduction in the H-NOX Family. J. Am. Chem. Soc 134, 2044–2046. [PubMed: 22257139]

(3). Hossain S, and Boon EM (2017) Discovery of a novel nitric oxide binding protein and nitric oxide-responsive signaling pathway in Pseudomonas aeruginosa. ACS Infect. Dis 3, 454–461. [PubMed: 28238256]

(4). Hossain S, Heckler I, and Boon EM (2018) Discovery of a Nitric Oxide Responsive Quorum Sensing Circuit in Vibrio cholerae. ACS Chem. Biol 13, 1964–1969. [PubMed: 30060647]

(5). Borziak K, and Zhulin IB (2007) FIST: a sensory domain for diverse signal transduction pathways in prokaryotes and ubiquitin signaling in eukaryotes. Bioinformatics 23, 2518–21. [PubMed: 17855421]

(6). D'Argenio DA, and Miller SI (2004) Cyclic di-GMP as a bacterial second messenger. Microbiology 150, 2497–2502. [PubMed: 15289546]

(7). Bacon BA, Liu Y, Kincaid JR, and Boon EM (2018) Spectral Characterization of a Novel NO Sensing Protein in Bacteria: NosP. Biochemistry 57, 6187–6200. [PubMed: 30272959]

(8). Plate L, and Marletta M. a. (2012) Nitric oxide modulates bacterial biofilm formation through a multicomponent cyclic-di-GMP signaling network. Mol. Cell 46, 449–460. [PubMed: 22542454]

(9). Thormann KM, Saville RM, Shukla S, Pelletier DA, and Spormann AM (2004) Initial Phases of biofilm formation in Shewanella oneidensis MR-1. J. Bacteriol 186, 8096–8104. [PubMed: 15547283]

(10). Liu N, Xu Y, Hossain S, Huang N, Coursolle D, Gralnick JA, and Boon EM (2012) Nitric Oxide Regulation of Cyclic di-GMP Synthesis and Hydrolysis in Shewanella woodyi. Biochemistry 51, 2087–2099. [PubMed: 22360279]

(11). Godeke J, Paul K, Lassak J, and Thormann KM (2011) Phage-induced lysis enhances biofilm formation in Shewanella oneidensis MR-1. ISME J. 5, 613–626. [PubMed: 20962878]

(12). Besharova O, Suchanek VM, Hartmann R, Drescher K, and Sourjik V (2016) Diversification of Gene Expression during Formation of Static Submerged Biofilms by Escherichia coli. Front. Microbiol, 1568.

(13). Singh PK, Bartalomej S, Hartmann R, Jeckel H, Vidakovic L, Nadell CD, and Drescher K (2017) Vibrio cholerae Combines Individual and Collective Sensing to Trigger Biofilm Dispersal. Curr. Biol 27, 3359–3366. [PubMed: 29056457]

(14). Otsu N (1979) A Threshold Selection Method from Gray-Level Histograms. IEEE Trans. Syst. Man. Cybern 9, 62–66.

(15). Driscoll WC (1996) Robustness of the ANOVA and Tukey-Kramer Statistical Tests. Comput. Ind. Eng 31, 265–268.

(16). Burhenne H, and Kaever V (2013) Quantification of cyclic dinucleotides by reversed-phase LC-MS/MS. Methods Mol. Biol 1016, 27–37. [PubMed: 23681570]

(17). Bradford MM (1976) A rapid and sensitive method for the quantitation of microgram quantities of protein utilizing the principle of protein-dye binding. Anal. Biochem 72, 248–254. [PubMed: 942051]

(18). Price MS, Chao L, and Marletta MA (2007) Shewanella oneidensis MR-1 H-NOX Regulation of a Histidine Kinase by Nitric Oxide. Biochemistry 46, 13677–13683. [PubMed: 17988156]

(19). Boon EM, Davis JH, Tran R, Karow DS, Huang SH, Pan D, Miazgowicz MM, Mathies R. a, and Marletta M. a. (2006) Nitric oxide binding to prokaryotic homologs of the soluble guanylate cyclase beta1 H-NOX domain. J. Biol. Chem 281, 21892–21902. [PubMed: 16728401]

(20). Kharitonov VG, Sharma VS, Magde D, and Koesling D (1997) Kinetics of Nitric Oxide Dissociation from Five- and Six-Coordinate Nitrosyl Hemes and Heme Proteins, Including Soluble Guanylate Cyclase. Biochemistry 36, 6814–6818. [PubMed: 9184164]

(21). Rueden CT, Schindelin J, Hiner MC, DeZonia BE, Walter AE, Arena ET, and Eliceiri KW (2017) ImageJ2: ImageJ for the next generation of scientific image data. BMC Bioinf. 18, 529.

(22). Fredrickson JK, Romine MF, Beliaev AS, Auchtung JM, Driscoll ME, Gardner TS, Nealson KH, Osterman AL, Pinchuk G, Reed JL, Rodionov DA, Rodrigues JLM, Saffarini DA, Serres MH, Spormann AM, Zhulin IB, and Tiedje JM (2008) Towards environmental systems biology of Shewanella. Nat. Rev. Microbiol 6, 592–603. [PubMed: 18604222]

(23). Ueno TB, Johnson RA, and Boon EM (2015) Optimized assay for the quantification of histidine kinase autophosphorylation. Biochem. Biophys. Res. Commun 465, 331–337. [PubMed: 26255967]

(24). Fisher SL, Kim SK, Wanner BL, and Walsh CT (1996) Kinetic comparison of the specificity of the vancomycin resistance kinase VanS for two response regulators, VanR and PhoB. Biochemistry 35, 4732–4740. [PubMed: 8664263]

(25). Grimshaw CE, Huang S, Hanstein CG, Strauch MA, Burbulys D, Wang L, Hoch JA, and Whiteley JM (1998) Synergistic kinetic interactions between components of the phosphorelay controlling sporulation in Bacillus subtilis. Biochemistry 37, 1365–1375. [PubMed: 9477965]

(26). Skerker JM, Prasol MS, Perchuk BS, Biondi EG, and Laub MT (2005) Two-component signal transduction pathways regulating growth and cell cycle progression in a bacterium: A systemlevel analysis. PLoS Biol. 3, e334. [PubMed: 16176121]

(27). Laub MT, Biondi EG, and Skerker JM (2007) Phosphotransfer profiling: systematic mapping of two-component signal transduction pathways and phosphorelays. Methods Enzymol. 423, 531–548. [PubMed: 17609150]

(28). Beier D, and Gross R (2006) Regulation of bacterial virulence by two-component systems. Curr. Opin. Microbiol 9, 143–152. [PubMed: 16481212]

(29). Arora DP, and Boon EM (2012) Nitric oxide regulated two-component signaling in Pseudoalteromonas atlantica. Biochem. Biophys. Res. Commun 421, 521–526. [PubMed: 22521885]

(30). Elsen S, Duche O, and Colbeau A (2003) Interaction between the H 2 Sensor HupUV and the Histidine Kinase HupT Controls HupSL Hydrogenase Synthesis in Rhodobacter capsulatus. J. Bacteriol 185, 7111–7119. [PubMed: 14645270]

(31). Szurmant H, Bu L, Brooks CL III, and Hoch JA (2008) An essential sensor histidine kinase controlled by transmembrane helix interactions with its auxiliary proteins. Proc. Natl. Acad. Sci. U. S. A 105, 5891–5896. [PubMed: 18408157]

(32). Rao M, Herzik MA, Iavarone AT, and Marletta MA (2017) Nitric Oxide-Induced Conformational Changes Govern H-NOX and Histidine Kinase Interaction and Regulation in Shewanella oneidensis. Biochemistry 56, 1274–1284. [PubMed: 28170222]

(33). Sinclair PR, Gorman N, and Jacobs JM (1999) Measurement of Heme Concentration. Curr. Protoc. Toxicol 8, 8.3.1–8.3.7.

(34). Giovannetti R (2012) The Use of Spectrophotometry UV-Vis for the Study of Porphyrins In Macro to Nano Spectroscopy (Uddin J, Ed.) pp 87–108, InTech.

(35). Maragos CM, Morley D, Wink DA, Dunams TM, Saavedra JE, Hoffman A, Bove AA, Isaac L, Hrabie JA, and Keefer LK (1991) Complexes of ' NO with Nucleophiles as Agents for the Controlled Biological Release of Nitric Oxide. Vasorelaxant Effects. J. Med. Chem 34, 3242–3247. [PubMed: 1956043]

(36). Stone JR, and Marletta MA (1996) Spectral and kinetic studies on the activation of soluble guanylate cyclase by nitric oxide. Biochemistry 35, 1093–1099. [PubMed: 8573563]

(37). Wu G, Liu W, Berka V, and Tsai A-L (2017) Gaseous ligand selectivity of the H-NOX sensor protein from Shewanella oneidensis and comparison to those of other bacterial H-NOXs and soluble guanylyl cyclase. Biochimie 140, 82–92. [PubMed: 28655588]

(38). Carlson HK, Vance RE, and Marletta M. a. (2010) H-NOX regulation of c-di-GMP metabolism and biofilm formation in Legionella pneumophila. Mol. Microbiol 77, 930–942. [PubMed: 20572940]

(39). Tsai A-L, Martin E, Berka V, and Olson JS (2012) How do heme-protein sensors exclude oxygen? Lessons learned from cytochrome c', Nostoc puntiforme heme nitric oxide/oxygen-binding domain, and soluble guanylyl cyclase. Antioxid. Redox Signaling 17, 1246–1263.

(40). Gilbert HF (2006) Molecular and cellular aspects of thioldisulfide exchange. Adv. Enzymol. Relat. Areas Mol. Biol 63, 69–172.

(41). Ziegler DM, and Poulsen LL (1977) Protein disulfide bond synthesis: a possible intracellular mechanism. Trends Biochem. Sci 2, 79–81.

(42). Plate L, and Marletta M. a. (2013) Phosphorylationdependent derepression by the response regulator HnoC in the Shewanella oneidensis nitric oxide signaling network. Proc. Natl. Acad. Sci. U. S. A 110, E4648–E4657. [PubMed: 24218564]

(43). Henares BM, Higgins KE, and Boon EM (2012) Discovery of a Nitric Oxide Responsive Quorum Sensing Circuit in Vibrio harveyi. ACS Chem. Biol 7, 1331–1336. [PubMed: 22606970]

(44). Lahiri T, Luan B, Raleigh DP, and Boon EM (2014) A structural basis for the regulation of an H-NOX-associated cyclic-di-GMP synthase/phosphodiesterase enzyme by nitric oxide-bound H-NOX. Biochemistry 53, 2126–2135. [PubMed: 24628400]

(45). Rao M, Smith BC, and Marletta A (2015) Nitric Oxide Mediates Biofilm Formation and Symbiosis in Silicibacter. mBio 6, n/a.

(46). McCarter LL, and Gomelsky M (2015) Fifty ways to inhibit motility via cyclic di-GMP: The emerging Pseudomonas aeruginosa swarming story. J. Bacteriol 197, 406–409. [PubMed: 25448814]

(47). Thormann KM, Duttler S, Saville RM, Hyodo M, Shukla S, Hayakawa Y, and Spormann AM (2006) Control of Formation and Cellular Detachment from Shewanella oneidensis MR-1 Biofilms by Cyclic di-GMP. J. Bacteriol 188, 2681–2691. [PubMed: 16547056]

(48). Nair HAS, Periasamy S, Yang L, Kjelleberg S, and Rice SA (2017) Real Time, Spatial, and Temporal Mapping of the Distribution of c-di-GMP during Biofilm Development. J. Biol. Chem 292, 477–487. [PubMed: 27899451]

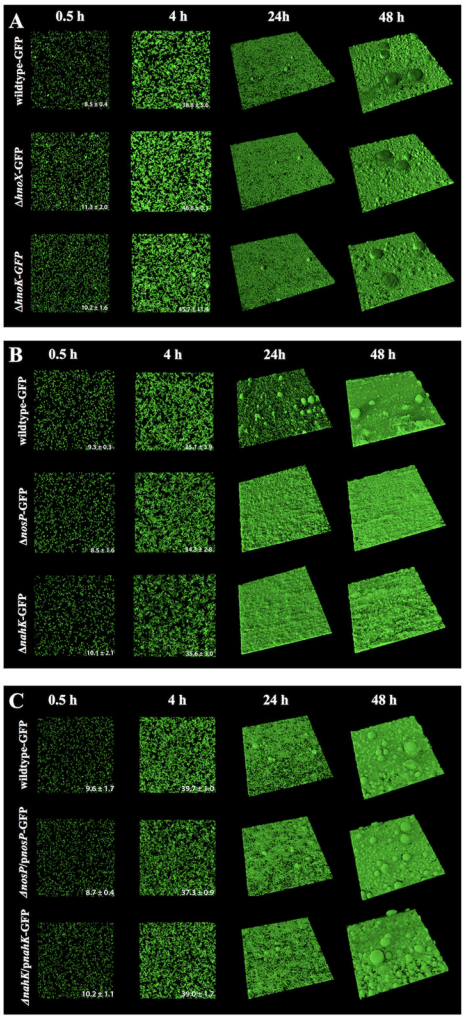

Figure 1.

*So*NosP and *So*NahK are essential for mature biofilm formation in *S. oneidensis*. (A) CSLM image projections of flow-cell biofilms of *S. oneidensis* wild-type GFP, Δ*hnoX*-GFP, and Δ*hnoK*-GFP strains. All mutants displayed wild-type biofilm phenotypes. (B) Flow-cell biofilms of *S. oneidensis* Δ*nosP*-GFP and Δ*nahK*-GFP strains displayed monolayer biofilm phenotypes at the 24 h time point. No micro- or macrocolony biofilm phenotypes were observed at the 24 or 48 h time points as in the wild-type strain. (C) Flow-cell biofilms of *S. oneidensis* Δ*nosP*-GFP and Δ*nahK*-GFP complement strains demonstrate restoration of the wild-type biofilm phenotype. Images after 0.5 and 4 h are top views; the lateral edge of the micrograph is 250 μm. The images after 24 and 48 h are shadow projections; the lateral edge is 775 μm. The numbers in the 0.5 and 4 h images display the surface coverage.

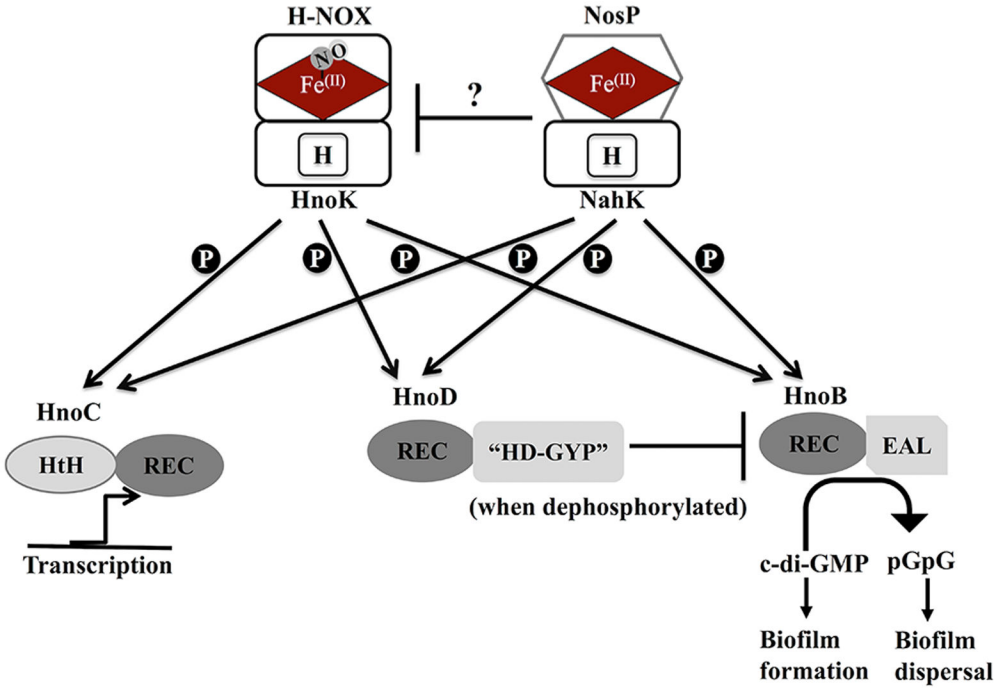

Figure 2.

*So*NosP is a master regulator of the multicomponent *S. oneidensis* c-di-GMP signaling network. We hypothesize that the NosP/NahK signaling pathway inhibits the H-NOX/HnoK signaling pathway, which not only leads to a change in phosphate flux to the three response regulators (HnoB, HnoC, and HnoD) but also ultimately results in a change in the intracellular levels of c-di-GMP and therefore biofilm formation in *S. oneidensis* via the modulation of HnoB phosphodiesterase activity.

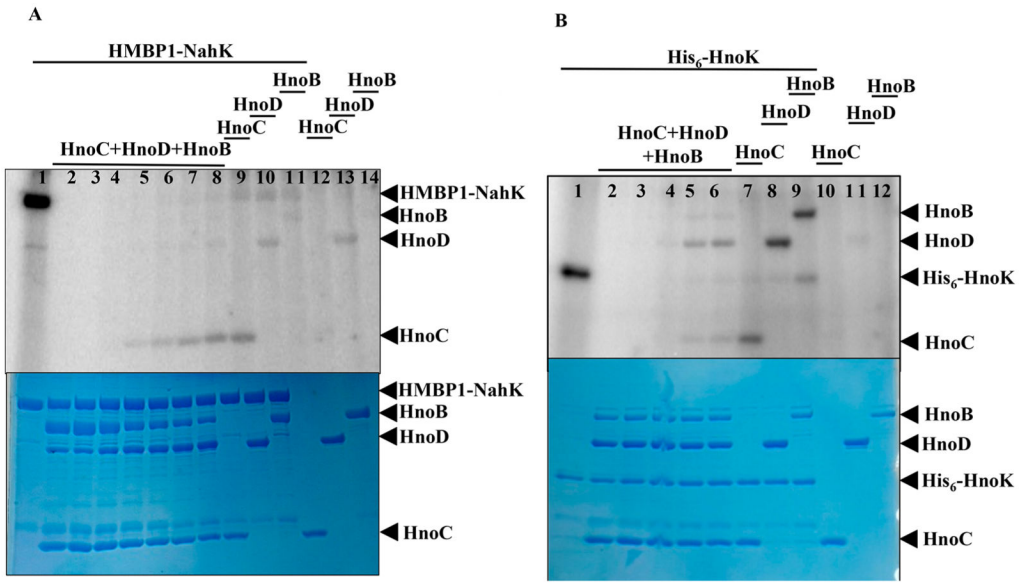

Figure 3.

*So*HnoK and *So*NahK exhibit kinetic preferences for different response regulator proteins *in vitro* in the absence of H-NOX and NosP. Radiolabeled phosphoproteins were detected by SDS–PAGE (bottom panel, indicating protein loading) and autoradiography (top panel, indicating phosphorylation). (A) *So*NahK displays a time-dependent kinetic preference for the HtH response regulator HnoC when all three response regulators (HnoB, HnoC, and HnoD) are present *in vitro*. Lane 1 represents *So*NahK (3 μM) incubated with radiolabeled ATP for 60 min. In lanes 2–8, SoNahK (3 μM) was preincubated with equimolar amounts of HnoB, HnoC, and HnoD simultaneously; radiolabeled ATP was then added, and aliquots were removed at various time points (0, 0.5, 2, 10, 15, 30, and 60 min) to assess which response regulator would become preferentially phosphorylated over time. Lanes 9–11 represent *So*NahK incubated with radiolabeled ATP with HnoC, HnoD, and HnoB, respectively. Lanes 12–14 represent radiolabeled ATP incubated with HnoC, HnoD, HnoB, respectively. (B) *So*HnoK displays a time-dependent kinetic preference for the HD-GYP response regulator HnoD when all three response regulators (HnoB, HnoC, and HnoD) are present *in vitro*. Lane 1 represents *So*HnoK (3 μM) incubated with radiolabeled ATP for 15 min. In lanes 2–6, *So*HnoK (3 μM) was preincubated with equimolar amounts of HnoB, HnoC, and HnoD simultaneously; radiolabeled ATP was then added, and aliquots were removed at various time points (0, 0.5, 2, 10, and 15 m) to assess which response regulator would become preferentially phosphorylated over time. Lanes 7–9 represent *So*HnoK incubated with radiolabeled ATP with HnoC, HnoD, and HnoB, respectively. Lanes 10–12 represent radiolabeled ATP incubated with HnoC, HnoD, and HnoB, respectively.

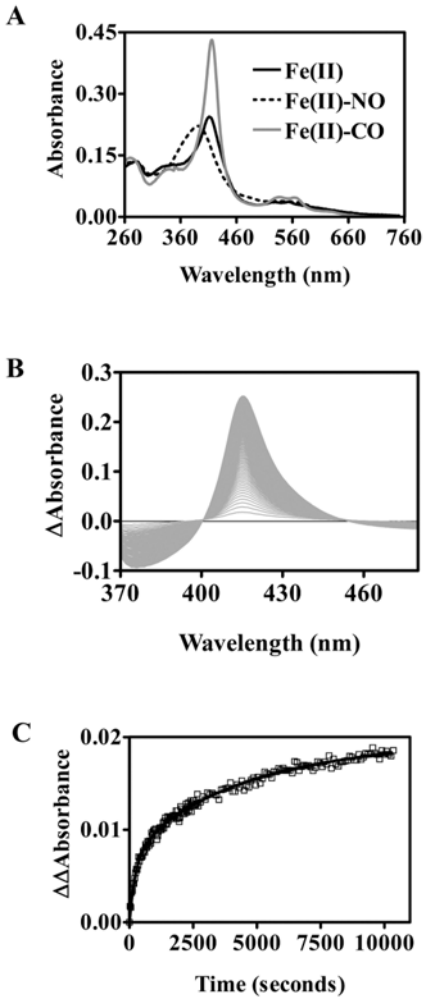

Figure 4.

*So*NosP displays ligand binding properties consistent with a NO sensor. (A) The UV–vis absorption spectrum of the ferrous form of *So*NosP [Fe(II)-unligated] displays a Soret maximum at 417 nm and split α/β bands at 552 and 524 nm (black solid line). The spectrum of the NO-bound ferrous form of *So*NosP [Fe(II)-NO] exhibits a Soret maximum at 397 nm (black dashed line). The spectrum of the CO-bound ferrous form of *So*NosP [Fe(II)-CO] displays a Soret maximum at 416 nm (gray solid line). (B) The rate constant for dissociation of NO from *So*NosP was measured using CO and 30 mM dithionite as a trap for released NO. A NO dissociation rate constant [k_{off}(NO)] of (2.25 ± 0.5) × 10^{-4} s^{-1} was measured for *So*NosP and is independent of CO and all dithionite concentrations used (3, 30, and 300 mM dithionite). A representative plot of the change in absorbance between the spectrum at each time point after addition of the CO/dithionite trap and the spectrum at 0 min. (C) Plot of the exponential fit of the data obtained by subtracting the difference in the absorbance at 397 nm [Fe(II)-NO *So*NosP] from the absorbance at 416 nm [Fe(II)-CO *So*NosP].

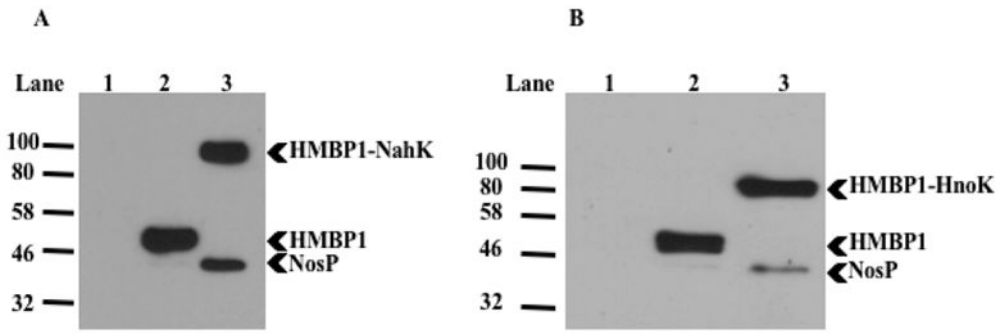

Figure 5.

NO-bound *So*NosP interacts with both *So*HnoK and *So*NahK. (A) Precipitation of NO-bound *So*NosP by HMBP1-*So*NahK. The His_6-tagged MBP fusion of *So*NahK (abbreviated as HMBP1-*So*NahK) was used to precipitate purified His_6-tagged SoNosP. HMBP1-*So*NahK (~100 kDa), HMBP1 (~50 kDa), and NO-bound SoNosP (~43 kDa) were all detected via an anti-His Western blot. The blot shows that NO/*So*NosP does not pull down with amylose resin (lane 1) or with HMBP1 alone (lane 2). NO/*So*NosP pull down can be detected only in the presence of HMBP1-*So*NahK (lane 3). (B) Precipitation of *So*NosP by HMBP1-*So*HnoK. The His_6-tagged MBP fusion of *So*HnoK (abbreviated as HMBP1-*So*HnoK) was used to precipitate purified His_6-tagged SoNosP. HMBP1-*So*HnoK (~80 kDa), HMBP1 (~50 kDa), and NO-bound SoNosP (~43 kDa) were all detected via an anti-His Western blot. The blot shows that NO/*So*NosP pull down is not detected in the presence of amylose resin only (lane 1) or HMPB1 alone (lane 2). NO/NosP pull down can be detected only in the presence of HMBP1-*So*HnoK (lane 3).

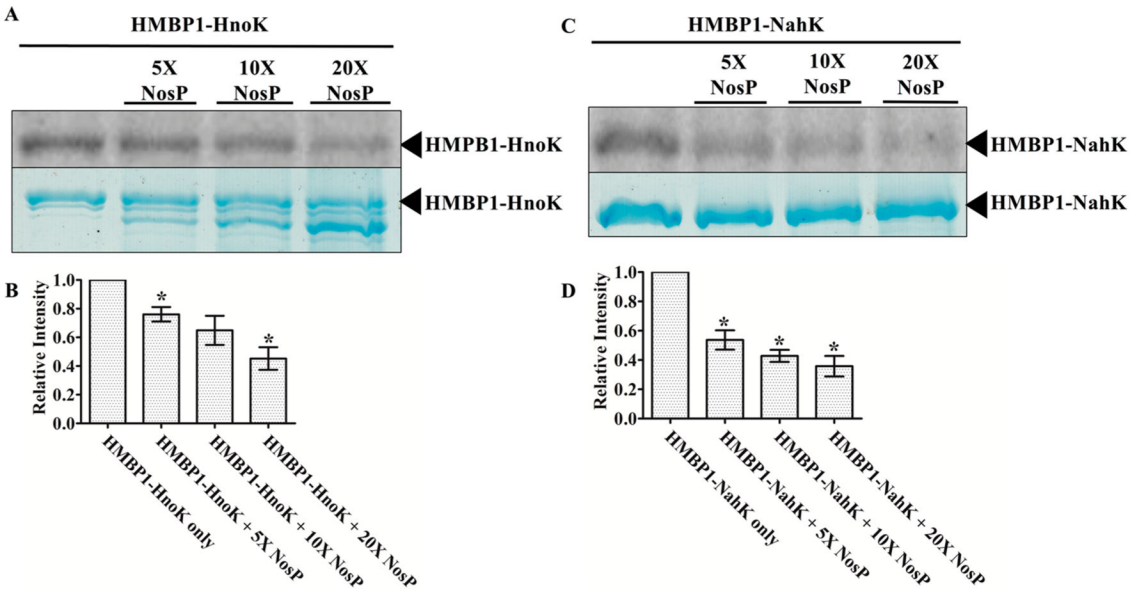

Figure 6.

Ferrous-unligated *So*NosP inhibits both *So*HnoK and *So*NahK autophosphorylation activity. Radiolabeled phosphoproteins were detected by SDS–PAGE (A and C, bottom panel, indicating protein loading) and autoradiography (A and C, top panel, indicating phosphorylation). (A) Fe(II)-unligated *So*NosP inhibits HnoK autophosphorylation activity in a concentration-dependent manner. *So*HnoK (3 μM) was incubated with radiolabeled ATP and varying amounts of ferrous-unligated *So*NosP (15, 30, and 60 μM), resulting in an Fe(II)/*So*NosP dose-dependent decrease in *So*HnoK autophosphorylation activity (top panel). (B) Intensity of phosphorylated *So*HnoK as a function of various Fe(II)/*So*NosP concentrations plotted vs the intensity of *So*HnoK autophosphorylation in the absence of Fe(II)/*So*NosP. (C) Fe(II)-unligated *So*NosP inhibits *So*NahK autophosphorylation activity in a concentration-dependent manner. *So*NahK (3 μM) was incubated with radiolabeled ATP and varying amounts of ferrous-unligated *So*NosP (15, 30, and 60 μM), resulting in an Fe(II)/*So*NosP dose-dependent decrease in *So*NahK autophosphorylation activity (top panel). (D) Intensity of phosphorylated *So*NahK as a function of various Fe(II)/*So*NosP concentrations plotted vs the intensity of *So*NahK autophosphorylation in the absence of Fe(II)/*So*NosP. Error bars represent the standard error of the mean of triplicate experiments. An asterisk denotes $p \leq 0.05$ compared to the relative intensity of wild-type histidine kinase autophosphorylation activity.

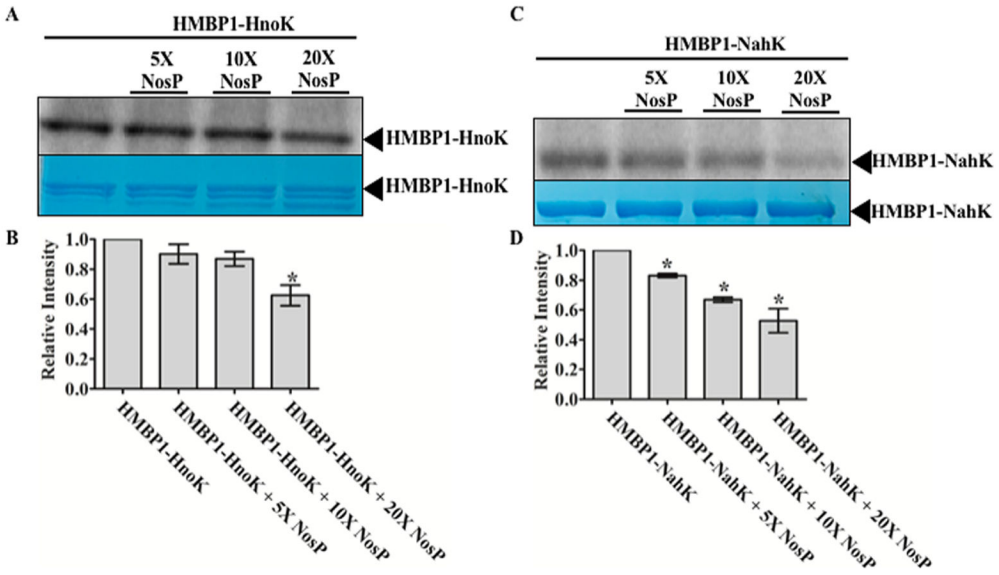

Figure 7.

NO-bound *So*NosP inhibits both *So*HnoK and *So*NahK autophosphorylation activity. Radiolabeled phosphoproteins were detected by SDS–PAGE (A and C, bottom panel, indicating protein loading) and autoradiography (A and C, top panel, indicating phosphorylation). (A) A NO/*So*NosP dose-dependent decrease in *So*HnoK autophosphorylation activity was observed. *So*HnoK (3 μM) was incubated with radiolabeled ATP and varying amounts of Fe(II)-NO *So*NosP (15, 30, and 60 μM), resulting in a NO/*So*NosP concentration-dependent decrease in *So*HnoK autophosphorylation activity (top panel). (B) Intensity of phosphorylated *So*HnoK as a function of various NO/*So*NosP concentrations plotted vs the intensity of *So*HnoK autophosphorylation in the absence of NO/*So*NosP. (C) A NO/*So*NosP dose-dependent decrease in *So*NahK autophosphorylation activity was observed. *So*NahK (3 μM) was incubated with radiolabeled ATP and varying amounts of Fe(II)-NO *So*NosP (15, 30, and 60 μM), resulting in a NO/*So*NosP concentration-dependent decrease in *So*NahK autophosphorylation activity (top panel). (D) Intensity of phosphorylated *So*NahK as a function of various NO/*So*NosP concentrations plotted vs the intensity of *So*NahK autophosphorylation in the absence of NO/*So*NosP. Error bars represent the standard error of the mean of triplicate experiments. An asterisk represents $p \leq 0.05$ compared to the relative intensity of wild-type histidine kinase autophosphorylation activity.

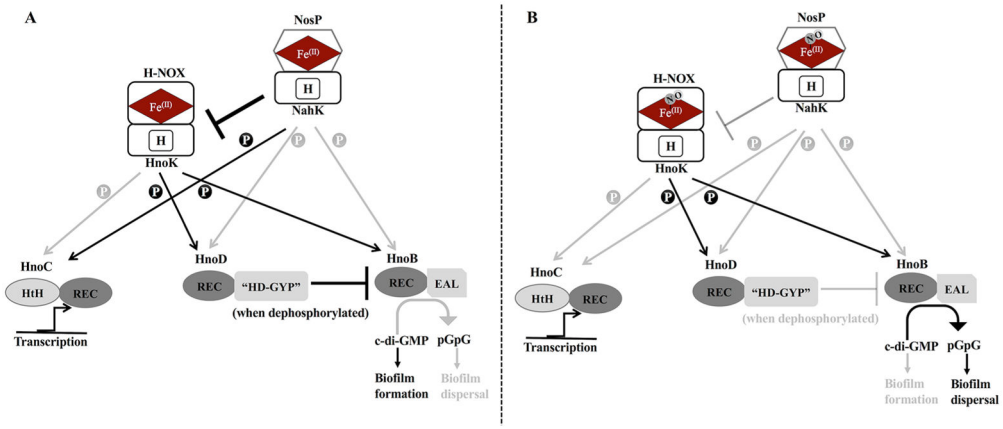

Figure 8.

*So*NosP is a master regulator of the multicomponent *S. oneidensis* c-di-GMP signaling network. *So*NosP and its associated signaling pathway are essential for regulating complex biofilm formation in *S. oneidensis*, and the molecular mechanism for this regulation is modulation of HnoB phosphodiesterase activity. (A) The ferrous-unligated *So*NosP/NahK signaling pathway strongly inhibits the H-NOX/HnoK signaling pathway. Ferrous-unligated H-NOX, however, has recently been demonstrated to downregulate HnoK autokinase activity. Consequently, the flux of phosphate to both HnoB and HnoD (darker arrows) significantly decreases, causing unphosphorylated HnoD to inhibit HnoB phosphodiesterase activity. This decrease in HnoB activity leads to increased levels of intracellular c-di-GMP and therefore complex biofilm production. (B) The NO-bound *So*NosP/NahK signaling pathway inhibits the H-NOX/HnoK signaling pathway. NO-bound H-NOX has previously been demonstrated to inhibit HnoK autokinase activity only in a large molar excess. As a result, the flux of phosphate to both HnoB and HnoD (darker arrows) occurs and the inhibition of HnoB phosphodiesterase activity is alleviated, leading to biofilm dispersal as phosphorylated HnoD does not inhibit HnoB activity. NahK displays a kinetic preference for HnoC (dark arrow, Figure 2A), which is a dedicated transcription factor that regulates gene transcription. From the data provided above, we can conclude that HnoC has no implications in regulating biofilm formation in this bacterium.

Table 1.

Student's *t* Test Statistical Analysis Data of Cellular c-Di-GMP Levels in *S. oneidensis*

	relative picomoles of c-di-GMP[a]		+NO relative to −NO	mutant strain −NO relative to MR-1−NO	mutant strain +NO relative to MR-1 +NO
strain	**−NO**	**+NO**	$p \leq 0.05$	$p \leq 0.05$	$p \leq 0.05$
MR-1	1	0.59 ± 0.1	yes[b]	N/A	N/A
Δ*hnoX*	0.95 ± 0.3	0.49 ± 0.1	no	no	no
Δ*hnoK*	0.81 ± 0.3	0.49 ± 0.1	no	no	no
Δ*nosP*	0.73 ± 0.1	0.46 ± 0.1	no	yes	no
Δ*nahK*	0.70 ± 0.1	0.57 ± 0.2	no	yes[b]	no
Δ*hnoB*	0.91 ± 0.1	0.81 ± 0.8	no	no	no
Δ*hnoD*	0.82 ± 0.2	0.49 ± 0.3	yes	no	no
Δ*hnoX*/Δ*nosP*	0.60 ± 0.2	0.37 ± 0.1	no	yes	no
Δ*hnoK*/Δ*nahK*	0.71 ± 0.2	0.37 ± 0.1	yes	no	yes
Δ*nosP*/p*nosP*	0.60 ± 0.2	0.28 ± 0.1	yes	N/A	N/A
Δ*nahK*/p*nahK*	0.53 ± 0.2	0.28 ± 0.2	yes[b]	N/A	N/A
Δ*hnoD*/p*hnoD*	0.56 ± 0.3	0.25 ± 0.1	no	N/A	N/A

[a] c-Di-GMP was normalized to the OD_{600} of the culture from which the c-di-GMP was extracted. The values reported here are relative to the c-di-GMP concentration of the wild-type MR-1 strain.

[b] $p \leq 0.01$.

Table 2.

Ligand Binding Properties of Some NO Binding Ferrous Hemoproteins[a]

	Soret band (nm)				
protein	**Fe(II)-unligated**	**Fe(II)-CO**	**Fe(II)-NO**	**k_{off}(NO) ($\times 10^{-4}$ s^{-1})**	**ref**
*So*NosP[b]	417	416	397	2.25 ± 0.5	this work
*Pa*NosP[c]	420	422	396	1.8 ± 0.5	3
sGC[d]	431	423	398	3.6 ± 0.9	36
*So*H-NOX[e]	427	424	398	0.13 ± 0.01	37
*Sw*H-NOX[f]	430	423	399	15.2 ± 3.5	10
*Lpg*H-NOX[g]	428	420	398	10.3 ± 1.4	38

[a] Soret band electronic absorption maxima and NO dissociation rate constants are listed.

[b] NosP from *S. oneidensis*.

[c] NosP from *P. aeruginosa*.

[d] H-NOX from bovine lung (H-NOX is one domain of sGC).

[e] H-NOX from *S. oneidensis*.

[f] H-NOX from *Shewanella woodyi*.

[g] H-NOX from *L. pneumophila*.